JOURNAL OF PETROLOGY | VOLUME 54 | NUMBER 12 | PAGES 2521–2545 | 2013 | doi:10.1093/petrology/egt055

The Temperature and Pressure Dependence of Nickel Partitioning between Olivine and Silicate Melt

ANDREW K. MATZEN*, MICHAEL B. BAKER, JOHN R. BECKETT AND EDWARD M. STOLPER

DIVISION OF GEOLOGICAL AND PLANETARY SCIENCES, CALIFORNIA INSTITUTE OF TECHNOLOGY, PASADENA, CA 91125, USA

RECEIVED AUGUST 29, 2012; ACCEPTED SEPTEMBER 5, 2013
ADVANCE ACCESS PUBLICATION OCTOBER 12, 2013

We measured Ni partitioning between olivine and melt, $D_{Ni}^{ol/liq}$, in experiments on mid-ocean ridge basalt (MORB) encapsulated in olivine at pressures from 1 atm to 3·0 GPa and temperatures from 1400 to 1550°C. We present a series of experiments where the temperature (T) at each pressure (P) was selected so that the liquid composition remained approximately constant over the entire P–T range. This approach allowed us to investigate the effects of T and P on $D_{Ni}^{ol/liq}$, independent of substantial changes in liquid composition. Our experiments show that for a liquid with ~18 wt % MgO, $D_{Ni}^{ol/liq}$ decreases from 5·0 to 3·8 as the temperature increases from 1400 to 1550°C. Fitting our experimental results and literature data to thermodynamic expressions for $D_{Ni}^{ol/liq}$ as a function of both temperature and liquid composition shows that the small variations in liquid composition in our experiments account for little of the observed variation of $D_{Ni}^{ol/liq}$. Because the changes in volume and heat capacity of the exchange reaction $MgSi_{0.5}O_2^{ol} + NiO^{liq} \leftrightarrow NiSi_{0.5}O_2^{ol} + MgO^{liq}$ are small, D_{Ni}^{molar}, the Ni partition coefficient on a molar basis, is well described by

$$ln\left(D_{Ni}^{molar}\right) = -\frac{\Delta_r H^{\circ}_{T_{ref},P_{ref}}}{RT} + \frac{\Delta_r S^{\circ}_{T_{ref},P_{ref}}}{R} - ln\left(\frac{X_{MgO}^{liq}}{X_{MgSi_{0.5}O_2}^{ol}}\right)$$

with $-\frac{\Delta_r H^{\circ}_{T_{ref},P_{ref}}}{R} = 4375\ K$ and $\frac{\Delta_r S^{\circ}_{T_{ref},P_{ref}}}{R} = -2{\cdot}023$ for our data ($-\frac{\Delta_r H^{\circ}_{T_{ref},P_{ref}}}{R} = 4338\ K$ and $\frac{\Delta_r S^{\circ}_{T_{ref},P_{ref}}}{R} = -1{\cdot}956$ for our experiments combined with a compilation of literature data). This expression is easy to use and applicable to a wide range of pressures, temperatures, and phase compositions. Based on our results and data from the literature, the temperature dependence of $D_{Ni}^{ol/liq}$ leads to the prediction that when a deep partial melt from a peridotitic mantle source is brought to low pressure and cooled, the first Mg-rich olivines to crystallize can have significantly higher NiO contents than those in the residual source from which the melt was extracted. This enrichment in Ni is driven by the difference between the temperature of low-pressure crystallization and the temperature of melt extraction from the residue. The average observed enrichment of Ni in forsteritic olivine phenocrysts from Hawaii—relative to the typical olivines from mantle peridotites—is consistent with a simple scenario of high-temperature partial melting of an olivine-bearing source at the base of the lithosphere followed by low-temperature crystallization of olivine. The most extreme enrichments of Ni in Hawaiian olivine phenocrysts and the lower Ni contents of some olivines can also be explained by the known variability of Ni contents of olivines from mantle peridotites via the same simple scenario. Although we cannot rule out alternative hypotheses for producing the high-Ni olivines observed in Hawaii and elsewhere, these processes or materials are unnecessary to account for NiO enrichments in olivine. The absolute temperature, in addition to the difference between the temperature of melt segregation from the residue and the temperature of low-pressure crystallization, is a significant factor in determining the degree of Ni enrichment in olivine phenocrysts relative to the olivines in the mantle source. The moderate Ni enrichment observed in most komatiitic olivines compared with those of Hawaii may result from the higher absolute temperatures required to generate MgO-rich komatiitic melts. Observed NiO enrichments in early crystallizing komatiitic olivine are consistent with their high temperatures of crystallization and with a deep origin for the komatiite parental melts.

*Corresponding author. Present address: Department of Earth Sciences, University of Oxford, Oxford OX1 3AN, UK. E-mail: andrew.matzen@earth.ox.ac.uk

KEY WORDS: *nickel partitioning; komatiite; Hawaii; olivine; ocean-island basalts*

INTRODUCTION

The study of the abundance and distribution of Ni within the Earth is a recurring theme in petrology and geochemistry because it can provide constraints on core formation and processes of accretion, partial melting, and low-pressure crystallization (e.g. Vogt, 1923; Ringwood, 1956; Häkli & Wright, 1967; Minarik *et al.*, 1996; Gaetani & Grove, 1997; Li & Ripley, 2010). It is the compatibility of Ni in olivine relative to silicate melt, which contrasts with the behavior of most other minor and trace elements, that makes it so useful in constraining igneous petrogenesis. For example, Hart & Davis (1978) showed that Ni contents of melts and coexisting olivine are sensitive to the fractionation of olivine and that high-MgO basalts from Baffin Island and Kilauea volcano are unlikely to be primary olivine-rich liquids; rather they reflect the accumulation of olivine. Another consequence of the compatibility of Ni in olivine relative to other phases in peridotites is that the Ni contents of residual olivine and bulk peridotites are relatively unaffected by the extraction of low degrees of partial melt (e.g. Mysen, 1978). Thus, if partial melting of the upper mantle is the main mechanism by which variations in its bulk composition are generated, olivines from mantle peridotites would be expected to display only a narrow range of Ni contents. This is, in fact, generally the case: observed olivines from spinel peridotites typically have 0·31–0·43 wt % NiO, with a median of 0·37 wt % (Korenaga & Kelemen, 2000).

Because the first olivine to crystallize from a partial melt of an olivine-bearing mantle source would be expected to closely approach the composition of residual olivine in the source, forsteritic olivine (i.e. early crystallizing) phenocrysts from basaltic magmas formed by partial melting of mantle peridotites are also expected to have Ni contents that are similar to those of olivines in their sources. These expectations are not always met. Olivines from some ocean islands (e.g. the Hawaiian islands) often have NiO contents exceeding 0·5 wt % (e.g. Clague *et al.*, 1991; Sobolev *et al.*, 2005, 2007), significantly higher than the olivines from peridotites. In contrast, forsteritic olivines from mid-ocean ridge basalt (MORB) can have significantly lower NiO contents; these are typically between 0·19 and 0·36 wt % (median is 0·28 wt %, with a maximum of 0·45 wt %; Sobolev *et al.*, 2007).

The unexpectedly large range of Ni contents in forsteritic olivine phenocrysts and the fact that this range extends beyond those commonly observed in mantle olivines has attracted considerable interest, given the apparent difficulty of generating high-Ni olivines by partially melting normal peridotitic mantle. Numerous alternatives have been proposed to explain the Ni-rich olivine phenocrysts. Ryabchikov (2003) suggested that the Ni content of the Hawaiian plume was elevated owing to interaction with the Earth's core, and Humayun & coworkers (Humayun *et al.*, 2004; Qin & Humayun, 2008) added support to this hypothesis via analyses of Fe/Mn ratios in MORB and ocean island basalt (OIB). Expanding on a model of Kelemen *et al.* (1998), Sobolev *et al.* (e.g. 2005, 2007) proposed that silica-rich partial melts of eclogite react with peridotite to form olivine-free pyroxenite. Their hypothesis states that in the absence of olivine, the bulk solid–liquid Ni partition coefficient for a pyroxenite is low, and consequently, high-Ni melts can be produced during subsequent partial melting of a metasomatized pyroxenite, resulting in the crystallization of Ni-rich olivines on ascent and cooling. Another possibility, proposed by Wang & Gaetani (2008), is that if a partial melt of an eclogite in equilibrium with olivine mixes with a tholeiitic liquid, high-Ni olivines can crystallize from relatively low-Ni melts owing to the control that liquid composition exerts on the olivine–liquid Ni partition coefficient (defined here as $D_{Ni}^{ol/liq} = NiO^{ol}/NiO^{liq}$, by weight). Alternatively, the partial melting of peridotites refertilized with MORB (e.g. Baker *et al.*, 2009) can produce melts that crystallize high-NiO olivines owing to the decrease in residual olivine and the corresponding decrease in the bulk Ni crystal–liquid partition coefficient (Shorttle & Maclennan, 2011). Finally, if $D_{Ni}^{ol/liq}$ is a function of temperature and pressure (e.g. Duke, 1976; Mysen & Kushiro, 1979), high-Ni olivines might crystallize on ascent and cooling of partial melts of 'normal' mantle peridotite (e.g. Matzen *et al.*, 2009; Li & Ripley, 2010; Niu *et al.*, 2011; Putirka *et al.*, 2011).

Our ability to quantitatively test these different possibilities requires characterizing the effects of pressure, temperature, melt composition, and fO_2 on $D_{Ni}^{ol/liq}$; that is, those variables that can change during generation, transportation, and crystallization of magmas. Although many experimental studies have been conducted to determine the partitioning of Ni between olivine and liquid, most were done at atmospheric pressure. For a given bulk composition at constant pressure, the temperature and the compositions of coexisting olivine and melt are strongly correlated (e.g. Wang & Gaetani, 2008; Herd *et al.*, 2009); this correlation makes it difficult to deconvolve the relative effects of temperature and composition on $D_{Ni}^{ol/liq}$ (e.g. Arndt, 1977; Hart & Davis, 1978; Takahashi, 1978). In the face of this difficulty, most researchers simply select temperature (e.g. Arndt, 1977; Hart & Davis, 1978; Kelemen *et al.*, 1998) or some aspect of the melt composition (commonly MgO; e.g. Hart & Davis, 1978) as the independent variable to model variations in $D_{Ni}^{ol/liq}$. Some researchers use $D_{Mg}^{ol/liq}$ as the independent variable (e.g. Jones, 1984; Beattie *et al.*, 1991; Beattie, 1993*a*); this is functionally equivalent to choosing either temperature or melt composition as the independent variable because $D_{Mg}^{ol/liq}$ is strongly

correlated with both temperature and melt composition. Models that parameterize $D_{Ni}^{ol/liq}$ using olivine and liquid compositions (e.g. Hart & Davis, 1978; Kinzler *et al.*, 1990; Beattie *et al.*, 1991) have gained wide acceptance owing to their ease of use and because the liquid composition during magmatic processes is generally more readily constrained than the temperature (e.g. Falloon *et al.*, 2007; Putirka *et al.*, 2007).

Models that describe $D_{Ni}^{ol/liq}$ in terms of liquid and olivine composition are generally successful at describing the available experimental data, but this success probably reflects the correlations between experimental run conditions and phase compositions. However, the covariations between these variables imposed by most experiments do not necessarily capture their covariations in nature. Even the simplest thermodynamic analysis indicates that $D_{Ni}^{ol/liq}$ depends on multiple independent variables: temperature, pressure, and the melt and mineral compositions (e.g. Leeman & Lindstrom, 1978; Kinzler *et al.*, 1990; Hirschmann & Ghiorso, 1994). If more than one of these variables are quantitatively important for processes in nature, models that do not separate their relative effects may yield a poor representation of those processes. The objective of this study is to constrain the temperature dependence of $D_{Ni}^{ol/liq}$ by conducting a series of experiments in which temperature and pressure covary in such a way that liquid and olivine compositions remain nearly constant. Observed differences in $D_{Ni}^{ol/liq}$ from such experiments must then reflect the effects of temperature (and pressure) rather than variations in phase chemistry. Preliminary reports on the work presented here have been given by Matzen *et al.* (2009, 2010).

EXPERIMENTAL METHODS

A basic design consideration for our experiments was the need to measure equilibrium Ni partitioning between basaltic liquids and olivine as a function of pressure and temperature at constant melt composition. In principle, this should be a simple matter: for a given melt composition, one need determine only the composition of the liquidus olivine as a function of pressure. Because the liquid composition is constant in such experiments (provided one could determine the olivine composition sufficiently close to the liquidus temperature), variations of $D_{Ni}^{ol/liq}$ would reflect only the effects of temperature and pressure. In practice, such experiments are not straightforward because in high-pressure experiments using the standard Pt–graphite, double-capsule technique, Ni is lost from the sample, passing through the graphite to the enclosing Pt capsule (e.g. J. Longhi, personal communication; A. Matzen, unpublished data). Graphite-only capsules also fail to retain Ni (e.g. Filiberto *et al.*, 2009).

To minimize Ni loss in our experiments, we surrounded a small chip of fused Juan de Fuca MORB glass (6·97 wt % MgO and <0·03 wt % NiO; see Table 1 for full analyses of all starting materials) with powdered Kilbourne Hole olivine [49·04 wt % MgO, Mg# = 90·2, where Mg# = Mg/(Mg + Fe) atomic, and 0·37 wt % NiO] in a Pt–graphite double capsule. In all of our experiments, the mass of the glass chip is small compared with that of the olivine, accounting for, on average, only 4% of the weight of all silicate material in a given capsule. Once in the piston cylinder, the capsule was sintered ~15°C below the solidus of the basalt for ~6 h (see Table 2 for run conditions) and slightly below the final run pressure (i.e. most experiments were hot–piston in; see Table 2), effectively transforming the powdered olivine into a polycrystalline olivine crucible that surrounds the melt and separates it from the graphite liner and outer Pt capsule. After sintering, the temperature was then increased to the final run temperature followed by a pressure increase to the final run pressure [see Supplementary Data Fig. S1a (Supplementary Data are available for downloading at http://www.petrology.oxfordjournals.org) for a backscattered electron (BSE) image of a typical run product]. The inner 'olivine crucible' is the important feature in our experiments because Ni diffuses much more slowly through olivine than through liquid, allowing the olivines and liquid in the center of the charge to exchange until reaching equilibrium without significant loss of Ni. Analysis of our run products shows that this strategy was successful in minimizing Ni loss from the melt: an ~100 μm rind of sintered olivine immediately adjacent to the C capsule showed evidence of Ni loss but the melt was typically ~200 μm from the edge of the graphite capsule. More importantly, mass-balance calculations (discussed below) show that NiO was conserved in the interior portions of the sample, demonstrating quantitatively the success of this approach.

We selected a specific set of pressures and temperatures so that the resulting liquid would have ~18 wt % MgO (17·1–18·9 wt %, excepting one experiment with 16·3 wt % MgO; see Table 3). Another way to describe the overall experimental approach is that at each pressure, the temperature was chosen such that the MORB glass dissolved approximately the same amount of Kilbourne Hole olivine, resulting in a liquid composition that was similar in all experiments. All of the high-pressure experiments were run in a Rockland Research piston cylinder apparatus using a CaF_2 assembly, straight-walled graphite heaters, crushable MgO spacers, and $W_3Re/W_{25}Re$ thermocouples housed either in mullite (at pressures ≤2·5 GPa) or two-bore alumina (at 3·0 GPa). To approach anhydrous conditions, the capsule was dried for ~3 h at 400°C after loading and before being welded shut; crushable MgO was dried for ~18 h at 1000°C. In addition to the Pt–graphite double-capsule experiments described above, we also ran one experiment in a Re-foil capsule (Run 9); this experiment had no C inner capsule, just powdered

Table 1: Starting compositions (in wt %)

Sample	*n*	SiO_2	TiO_2	Al_2O_3	Cr_2O_3	FeO*	MnO	MgO	CaO	Na_2O	K_2O	P_2O_5	NiO	Sum
TT152-21-35[1]		50·80	1·84	13·70	—	12·40	0·22	6·67	11·50	2·68	0·15	0·19	—	100·15
TT152-21-35[2]		50·92	2·02	13·71	—	12·56	0·19	7·11	10·88	2·63	0·16	—	—	100·17
Fused TT152-21-35[3]	3	50·45(7)[4]	1·91(3)	14·04(9)	b.d.l.	12·06(10)	0·21(2)	6·97(2)	11·05(5)	2·59(6)	0·16(1)	0·19(3)	b.d.l.	99·63
Fused TT152-21-35+Ni[5]	5	49·63(7)	1·92(3)	13·78(7)	b.d.l.	12·33(8)	0·22(1)	6·98(5)	10·97(9)	2·60(3)	0·16(1)	0·18(2)	0·99(4)	99·77
Kilbourne Hole olivine[6]	10	40·76(16)	—	0·01(1)	0·01(1)	9·34(10)	0·12(2)	49·49(21)	0·07(1)	—	—	—	0·39(2)	100·19
Kilbourne Hole olivine[7]	29	40·85(15)	b.d.l.	0·02(1)	0·02(1)	9·47(5)	0·14(1)	49·04(19)	0·08(1)	—	—	—	0·37(2)	99·99
San Carlos olivine[8]	4	40·47(6)	b.d.l.	0·02(2)	0·021(5)	9·17(29)	0·13(1)	49·03(33)	0·11(7)	—	—	—	0·39(3)	99·35

n, number of analyses used to generate the average. b.d.l., below detection limit; —, not analyzed or reported.
*All Fe as FeO.
[1]Composition as reported by Dixon *et al.* (1995).
[2]Composition as reported by Fine & Stolper (1986).
[3]Fused at 1 atm and 1240°C on a pre-doped Pt loop at QFM for 0·5 h.
[4]Numbers in parenthesis are analytical uncertainties in terms of the least units cited; for example, entry 50·45(7) for sample 'Fused TT152-21-35' corresponds to $50{\cdot}45 \pm 0{\cdot}07$ where 0·07 is the standard deviation of the three measurements made for this sample.
[5]Approximately 1 wt % NiO was mixed with TT152-21-35 glass powder and then fused at the same conditions as noted in footnote 3.
[6]Kilbourne Hole Olivine as reported by Wasylenki *et al.* (2003).
[7]Composition of Kilbourne Hole olivine powder used in experiments.
[8]San Carlos olivine capsule used in experiment 25 (Table 2).

Kilbourne Hole olivine encased in Re foil surrounding a MORB chip. For pressures at and below 2·5 GPa, turning off the power successfully produced a glass from the high-temperature melt; however, a quench mat formed in Run 30 (3·0 GPa) when this procedure was used; in subsequent 3·0 GPa experiments, we created analyzable glass pools using the pressure-drop quench technique of Putirka *et al.* (1996).

Experiments were also done at 1 atm in a Del-Tech VT-31 gas mixing furnace using methods similar to those of Wang & Gaetani (2008): crucibles of single crystal San Carlos olivine (49·0 wt % MgO, $Mg\# = 90{\cdot}5$, and 0·39 wt % NiO) were drilled to form a 2·5 mm diameter, ~2·5 mm deep cavity that was filled with a mixture of MORB and powdered Kilbourne Hole olivine and suspended by Pt wires (an image of a typical 1 atm run product is shown in Fig. S1b of the Supplementary Material). Oxygen fugacity was controlled using flowing H_2 and CO_2; low flow rates (~4·8 cm min^{-1}) were used to minimize alkali loss (e.g. Tormey *et al.*, 1987). The fO_2 was ~1·7 log units below the quartz–fayalite–magnetite (QFM) buffer, a value similar to that of estimates for the fO_2 of high-pressure experiments run in graphite capsules (QFM − 2·2; Médard *et al.*, 2008). For both the 1 atm and high-pressure experiments, in addition to the 'forward' experiments described above in which the NiO contents of the melt increased during the experiments, reversals were conducted by doping the starting MORB glass with ~1 wt % NiO (see Table 1).

Phase compositions are reported in Table 3; they were measured on Caltech's JEOL JXA-8200 electron microprobe and processed using a modified ZAF procedure (CITZAF; Armstrong, 1988). Glasses were initially analyzed at 15 keV using a 10 nA beam and a 10 μm spot, except for the quench mat of Run 30 for which a 20 μm diameter spot was used; on-peak counting times ranged from 30 to 60 s and half of that on each of the high and low backgrounds, respectively. Secondary glass standards (BHVO-2g, BIR-1g, and BCR-2g) were all analyzed during each microprobe session; the mean BHVO-2g composition from each session coupled with the accepted composition of BHVO-2 (http://minerals.cr.usgs.gov/geo.chem_stand/) was used to reprocess the k-ratios for all glass analyses from a session. In subsequent analytical sessions, Ni, Mn, and Cr were reanalyzed with a 200 nA beam, a 20 μm spot, and longer counting times (~90 s on peak and half of the on-peak counting time for each of the high and low backgrounds). These new data were then processed using the major and minor element concentrations from the low beam current analyses. This dual-pass technique provides a dataset that contains both analyses of beam-sensitive elements (e.g. Na_2O and K_2O) and high-precision analyses of NiO; per cent errors on the NiO content of the liquid average ~4% [where 'per cent error' = 100 × (standard deviation/mean)].

Olivine and pyroxene compositions were measured using a 1 μm spot, a 100 nA beam current and an accelerating voltage of 15 keV. On-peak counting times for olivines ranged from 20 s (Ti) to 140 s (Al); Ni was counted for 90 s. Olivine secondary standards (San Carlos and Guadeloupe) were repeatedly analyzed during each analytical session to monitor drift but no additional

Table 2: Run conditions and run products

Run no.	Final run conditions			Hot press conditions			Capsule[1]	Initial glass (wt %)	Run products[2]	Phase proportions[3] (wt %)	% NiO change[4] (relative)	*Q* value[5]	$D_{Ni}^{ol/liq}$[6]
	T (°C)	*P* (GPa)	*t* (h)	*T* (°C)	*P* (GPa)	*t* (h)							
6	1450	1·0	12·0	890	0·88	6·0	Pt-C	4·18	gl, ol	8·1, 91·9	-12·2	0·29	4·45(24)
7	1450	1·0	18·0	890	0·89	6·0	Pt-C	3·23	gl, ol	6·0, 94·0	-10·8	0·44	4·66(31)
8	1450	1·0	6·0	890	0·89	6·0	Pt-C	2·79	gl, ol	11·2, 88·8	+0·7	0·06	4·31(20)
9[7]	1500	2·0	12·2	940	1·89	6·3	Re	2·32	gl, ol	11·0, 89·0	+3·0	0·61	4·38(15)
10	1500	2·0	12·0	940	1·75	6·0	Pt-C	1·99	gl, ol, l-px	11·1, 88·9, 0	+3·2	0·99	4·35(17)
13	1525	2·5	12·0	965	2·20	6·0	Pt-C	3·25	gl, ol, l-px	24·8, 73·4, 1·8	+1·5	0·99	4·16(20)
17R	1450	1·0	12·0	890	0·89	6·0	Pt-C	5·24	gl, ol	6·7, 93·3	—	0·99	4·47(21)
25	1399	1×10^{-4}	8·0	—	—	—	SCOl	—	gl, ol	63·4, 36·6	-2·6	0·88	5·02(24)
28R[7]	1500	2·0	10·7	940	1·81	6·0	Pt-C	8·49	gl, ol, l-px	17·0, 83·0, 0	—	0·99	4·59(13)
30	1550	3·0	12·0	990	2·65	6·0	Pt-C	3·32	gl[8], ol, l-px	15·0, 82·0, 2·9	+5·9	0·70	3·82(29)
32R	1402	1×10^{-4}	8·0	—	—	—	SCOl	—	gl, ol	96·9, 3·1	—	0·13	4·94(12)
33R	1550	3·0	12·0	990	2·70	6·1	Pt-C	12·26	gl, ol, l-px, h-px	52·4, 28·0, 2·7, 16·9	—	0·99	3·73(18)
45R	1450	1·0	12·2	915	1·50	16·4	Pt-C	2·45	gl, ol	6·2, 93·8	—	0·40	4·57(24)

Run number followed by the letter R denotes a reversal experiment. The 1 atm experiments, runs 25 and 32R, were conducted at fO_2 values ~1·7 log units below the QFM buffer ($\log_{10} fO_2 = -8{\cdot}07$ and $-8{\cdot}09$, respectively); relative change in bulk Na_2O for these two experiments: $-20{\cdot}0$ and $+4{\cdot}9$% of the initial Na_2O content. Hot press conditions are not applicable to the 1 atm experiments.
[1]Capsule abbreviations: Pt-C, platinum–graphite double capsule; Re, Re-foil capsule; SCOl, San Carlos Olivine.
[2]Run product abbreviations: gl, glass (quenched liquid); ol, olivine; l-px, low-Ca pyroxene; h-px, higher-Ca pyroxene.
[3]Phase proportions, calculated by mass balance, are given in the same order as listed in the run products column.
[4]Relative change (in per cent) of NiO from the bulk composition based on mass balance; negative sign denotes a decrease whereas a positive sign indicates an increase in the NiO content of the bulk. Values are not reported for the reversal experiments where NiO in the olivine is strongly zoned towards the rims leading to positive '% NiO change' values that are a numerical artifact of this zoning (see text for further discussion).
[5]Goodness of fit measure; values above 0·05 indicate a solution acceptable at the 95% confidence level.
[6]Measured olivine–liquid Ni partition coefficient, by weight. Number in parenthesis represents the analytical uncertainty according to the least units cited; for example, 4·45(24) represents $4{\cdot}45 \pm 0{\cdot}24$. Error reflects the propagated analytical uncertainty (one sample standard deviation) of NiO in the olivine and glass (Table 3).
[7]Upon heating to the final-run temperature, pressure increased above the desired final-run pressure. Pressure was slowly bled off until final run-pressure was reached. Thus, these two experiments were hot-piston out; all other runs were hot-piston in.
[8]Quench mat.

corrections were applied. Transects made across near-melt olivines (typically ~20–100 μm in diameter) from forward experiments reveal uniform NiO concentrations. Most of the analyses reported in Table 3 were collected ~10 μm from the edge of the olivine–glass interface. Near-melt olivines in reversal experiments are, however, zoned in Ni, with NiO decreasing from core to rim. In an effort to capture the equilibrium $D_{Ni}^{ol/liq}$ for the reversal experiments, we performed a series of analyses with small step sizes (~2–4 μm) approaching the ol–liq interface and report (Table 3) the NiO contents of the analytical point closest to the interface that did not show contamination from the glass phase, which we took to be Al_2O_3 concentrations exceeding 150% of the value in the core of the olivine. Excepting NiO, all reversal-experiment olivine concentrations and all uncertainties (i.e. including NiO) come from the average and the standard deviation from data points collected ~10 μm from the edge of the olivine–glass interface. For all experiments, our analytical procedures lead to errors of ~3% relative for the NiO contents in the olivines. Using the standard deviations reported in Table 3, the resulting uncertainty (or error as defined above) on the measured $D_{Ni}^{ol/liq}$ is ~5%.

EXPERIMENTAL RESULTS

Phase compositions

Glass

Ideally, the composition of the melt in each of our experiments represents that of the initial MORB glass perturbed by the dissolution of and exchange with surrounding Kilbourne Hole or San Carlos olivine (see Table 1 for compositions of starting materials), with the amount of dissolution at any pressure dictated by the temperature. Because our objective was to evaluate $D_{Ni}^{ol/liq}$ at a constant liquid composition, we explicitly chose a run temperature for each pressure (Table 2) that would lead to dissolution of approximately the same amount of olivine and yield a

Table 3: Phase compositions

Run	ph	*n*	SiO_2	TiO_2	Al_2O_3	Cr_2O_3[1]	FeO*	MnO	MgO	CaO	Na_2O	K_2O	P_2O_5	NiO[1]	Sum
6	gl	9	49·91(15)	1·41(4)	11·10(10)	0·015(1)	10·73(7)	0·20(2)	17·66(8)	7·41(4)	1·95(2)	0·12(1)	0·11(2)	0·073(3)	100·7
	ol	10	40·74(17)	0·022(4)	0·070(4)	0·013(3)	9·94(4)	0·14(1)	48·56(19)	0·21(1)	—	—	—	0·324(8)	100·0
7	gl	7	50·18(7)	1·44(2)	11·29(7)	0·014(2)	10·31(9)	0·19(2)	17·36(3)	7·18(3)	1·98(3)	0·13(1)	0·13(2)	0·071(4)	100·3
	ol	9	40·50(16)	0·02(1)	0·069(3)	0·013(2)	9·86(4)	0·14(1)	48·50(11)	0·20(1)	—	—	—	0·329(12)	99·6
8	gl	10	49·57(15)	1·45(3)	11·20(8)	0·016(1)	10·66(7)	0·21(2)	17·40(9)	7·56(4)	1·92(4)	0·12(1)	0·13(2)	0·086(4)	100·3
	ol	10	40·29(19)	0·018(3)	0·07(1)	0·013(4)	9·99(3)	0·14(1)	48·11(15)	0·22(1)	—	—	—	0·371(5)	99·2
9	gl	9	47·84(15)	1·34(4)	9·75(5)	0·019(2)	11·45(5)	0·20(2)	18·87(7)	7·93(5)	1·67(3)	0·12(1)	0·13(1)	0·087(3)	99·4
	ol	10	40·88(20)	0·009(4)	0·09(2)	0·011(2)	9·47(9)	0·13(1)	48·97(22)	0·21(2)	—	—	—	0·381(5)	100·2
10	gl	10	48·40(15)	1·47(3)	10·62(5)	0·016(1)	10·77(10)	0·19(2)	18·37(6)	7·75(3)	1·84(3)	0·14(1)	0·13(2)	0·088(3)	99·8
	ol	8	41·02(24)	0·01(1)	0·08(1)	0·010(3)	9·64(4)	0·136(4)	48·73(31)	0·204(4)	—	—	—	0·381(6)	100·2
	l-px	7	56·17(33)	0·13(3)	2·59(13)	0·05(1)	6·41(10)	0·13(1)	33·30(28)	1·30(12)	0·10(1)	—	—	0·15(2)	100·3
13	gl	8	47·19(13)	1·62(4)	11·32(6)	0·018(2)	10·76(7)	0·20(2)	17·18(9)	8·75(5)	2·11(5)	0·15(1)	0·17(3)	0·089(4)	99·6
	ol	7	41·03(12)	0·02(1)	0·14(6)	0·013(3)	9·83(4)	0·14(1)	47·92(24)	0·27(1)	—	—	—	0·370(7)	99·7
	l-px	9	55·10(32)	0·16(3)	4·09(62)	0·05(1)	6·63(30)	0·13(1)	31·75(52)	1·77(46)	0·19(3)	—	—	0·13(1)	100·0
17R	gl	10	49·34(15)	1·45(4)	11·11(10)	0·015(2)	10·61(6)	0·20(2)	17·77(8)	7·53(05)	1·99(4)	0·12(1)	0·14(2)	0·111(4)	100·4
	ol	6	40·95(8)	0·029(4)	0·070(3)	0·013(3)	9·55(2)	0·14(1)	48·51(13)	0·22(1)	—	—	—	0·497(16)	100·0
25	gl	10	48·26(17)	1·44(4)	10·51(6)	0·018(1)	11·55(6)	0·20(3)	18·09(7)	8·32(6)	1·55(3)	0·10(1)	0·12(2)	0·081(3)	100·2
	ol	7	41·07(18)	0·02(1)	0·04(1)	0·018(14)	9·38(4)	0·140(3)	48·84(28)	0·27(1)	—	—	—	0·408(10)	100·2
28R	gl	9	48·34(25)	1·57(3)	11·34(6)	0·017(1)	10·76(6)	0·21(2)	17·17(7)	8·43(4)	2·05(3)	0·15(1)	0·14(3)	0·170(4)	100·3
	ol	11	41·03(40)	0·02(1)	0·10(2)	0·011(2)	9·76(12)	0·143(4)	48·15(14)	0·25(1)	—	—	—	0·782(12)	100·2
	l-px	10	55·72(26)	0·16(2)	3·05(20)	0·05(1)	6·57(15)	0·13(1)	32·30(21)	1·59(5)	0·12(1)	—	—	0·35(5)	100·0
30	gl	11	46·38(91)	1·59(9)	10·92(18)	0·015(2)	11·65(1·01)	0·20(2)	18·28(80)	8·99(18)	1·62(38)	0·13(6)	0·17(4)	0·102(8)	100·1
	ol	7	41·14(5)	0·0016(2)	0·14(2)	0·008(3)	9·91(21)	0·140(5)	48·39(27)	0·25(4)	—	—	—	0·390(9)	100·4
	l-px	10	55·27(11)	0·15(3)	4·11(11)	0·04(1)	6·57(9)	0·13(1)	31·59(17)	2·01(6)	0·23(1)	—	—	0·13(1)	100·2
32R	gl	8	48·82(24)	1·44(3)	10·69(7)	b.d.l.	11·51(7)	0·20(2)	17·06(6)	8·46(5)	2·09(4)	0·11(1)	0·12(2)	0·418(7)	100·9
	ol	8	41·16(34)	0·022(5)	0·03(1)	0·018(3)	9·68(4)	0·147(3)	47·13(17)	0·26(2)	—	—	—	2·063(38)	100·5
33R	gl	9	45·40(38)	1·90(3)	11·76(6)	b.d.l.	12·40(7)	0·20(2)	16·31(8)	8·97(3)	2·31(4)	0·18(1)	0·18(1)	0·396(4)	100·0
	ol	9	41·00(5)	0·02(1)	0·15(3)	0·011(4)	11·30(22)	0·147(5)	46·71(32)	0·29(2)	—	—	—	1·476(68)	101·1
	l-px	10	54·30(29)	0·17(2)	5·27(34)	0·04(1)	7·10(6)	0·14(1)	29·99(25)	2·32(11)	0·31(2)	—	—	0·58(2)	100·2
	h-px	10	53·69(25)	0·21(4)	5·87(30)	0·05(1)	7·00(9)	0·17(1)	24·83(69)	6·83(42)	0·87(7)	—	—	0·59(5)	100·1
45R	gl	13	48·87(10)	1·44(3)	11·10(7)	0·023(1)	10·46(6)	0·20(2)	17·41(8)	7·19(4)	1·96(3)	0·13(1)	0·12(2)	0·134(3)	99·0
	ol	11	40·54(10)	0·019(5)	0·064(3)	0·016(2)	9·86(5)	0·14(1)	48·28(19)	0·20(1)	—	—	—	0·612(29)	99·7

All compositions listed in wt %. Phase (ph); other abbreviations as in Table 2. Numbers in parenthesis are analytical uncertainties in terms of the least units cited; for example, 49·91(15) corresponds to $49{\cdot}91 \pm 0{\cdot}15$ where 49·91 represents the average of *n* analyses, and 0·15 is one standard deviation of those analyses; when the error is $\geq$1·0, we include the decimal point. —, not analyzed; b.d.l., below detection limit.
*All Fe as FeO.
[1]Element in the glass phase was analyzed with a 200 nA beam current (see text). *n* for NiO concentrations in the glass is 12 for Run 30; 11 for Runs 25 and 45R; 10 for Runs 7 and 13; 9 for Runs 6, 8, 10 and 33R; and 8 for Runs 9, 17R, 28R and 32R.

melt with ~18 wt % MgO. Glass compositions (Table 3) were all in the range of 16–19 wt % MgO (11 of 13 were in the narrower 17·1–18·4 wt % range). As expected, glass compositions generally reflect dissolution and precipitation of olivine, but five of the 13 experiments (those run at the highest pressures) also contain pyroxene.

Silica contents vary from 50·1 to 45·4 wt % and decrease with increasing pressure (from 1 to 3 GPa). To first order, this variation reflects the appearance of pyroxene (with 54–56 wt % SiO_2; discussed in more detail below) in the 2–3 GPa experiments. Pyroxene saturation in our 2–3 GPa experiments (two of the three 2 GPa runs contain minor amounts of low-Ca pyroxene and pyroxene abundance increases with increasing pressure; see Table 2) is consistent with the well-known experimental observation that olivine-saturated basaltic liquids become pyroxene

saturated with increasing pressure (e.g. Elthon & Scarfe, 1984). The slightly lower silica contents of the 1 atm experimental glasses relative to the 1 GPa liquids reflect the differences in composition between San Carlos olivine, used for the 1 atm crucibles, and Kilbourne Hole olivine, used in the higher-pressure experiments (Table 1). The increase in liquid CaO content from 1 to 3 GPa also reflects the crystallization of low-Ca pyroxenes (and in the case of Run 30, a subcalcic clinopyroxene). Variable degrees of melt infiltration into the sintered olivine and, thus, interaction of melt with differing volumes of Kilbourne Hole olivine (with low initial CaO) from experiment to experiment may explain the more subtle variations in liquid CaO content in the 1 GPa runs. Based on mass balance, at constant liquid MgO content, the fraction of liquid is smaller when a liquid coexists with olivine and pyroxene than when it equilibrates with olivine alone. Thus, the slight and somewhat scattered increase in minor element contents in the experimental liquids probably reflects the increasing abundance of pyroxene with increasing pressure.

Despite the variations in melt composition described above, we judge that we achieved our basic objective of obtaining a roughly constant melt composition over a significant range of pressure and temperature. In the Supplementary Material, we show that the relatively small variations in glass composition observed in our experiments have little effect on $D_{Ni}^{ol/liq}$, especially compared with the systematic variation in $D_{Ni}^{ol/liq}$ we observe with increasing temperature and pressure.

Olivine

Olivine compositions vary little in our experiments (see Table 3), consistent with our experimental design. Excluding Run 33R (ol Mg# = 88·1), which crystallized large amounts of pyroxene (~18 wt %), the average Mg# values of the near-melt olivines span a narrow range, 89·6–90·3, bracketing the Mg# of the starting Kilbourne Hole olivine (90·2). In the high-pressure experiments, the CaO content of olivine near the melt pool in the center of the charge increases with pressure, from ~0·21 wt % at 1·0 GPa to ~0·26 wt % CaO at 3·0 GPa, qualitatively consistent with our inference that liquid interacts with a progressively smaller volume of low-Ca olivine because sintering at higher pressure minimizes infiltration of the olivine aggregate by the melt. Al_2O_3 in olivines adjacent to melt increases from 0·04 wt % at 1 atm to 0·15 wt % Al_2O_3 at 3·0 GPa. In our experiments, the Al_2O_3 olivine–liquid partition coefficient increases with increasing pressure and temperature and agrees well with the model of Agee & Walker (1990).

Pyroxene

Low-Ca pyroxene (1·3–2·3 wt % CaO) is in contact with the central melt pool in five of 13 experiments, and a subcalcic clinopyroxene (6·8 wt % CaO) in one of these five (Run 33R); these occurrences are listed in Table 2, and pyroxene compositions are listed in Table 3. The SiO_2 contents of the low-Ca pyroxenes are higher than those of the glasses and span a narrow range from 54 to 56 wt %. The CaO content of the low-Ca pyroxenes increases with temperature (e.g. Lindsley *et al.*, 1981; Davidson *et al.*, 1982) rising from ~1·3 wt % at 1500°C to ~2·3 wt % at 1550°C. The Na_2O contents of the low-Ca pyroxene increase from 0·1 to 0·3 wt % with increasing temperature and pressure in our experiments. Overall, the compositions of low-Ca pyroxenes from our experiments are similar to those produced in the experiments of Walter (1998) and Hesse & Grove (2003). The higher-Ca pyroxene has a similar SiO_2 and a slightly lower MgO content relative to the low-Ca pyroxenes; overall its composition is similar to the experimentally produced subcalcic clinopyroxenes of Yaxley (2000) and Salters *et al.* (2002).

Mass balance

As briefly described above, high-pressure experiments run in graphite-only or Pt–graphite double capsules can lose substantial amounts of Ni on timescales that are short relative to typical experimental run durations. Nickel loss is also a serious problem in experiments conducted using platinum loops or capsules. Hart & Davis (1978) showed that in their 1 atm experiments the loss of Ni from their samples to the supporting platinum loop or capsule could result in anomalously high $D_{Ni}^{ol/liq}$ values. Nickel is lost much faster from the liquid than the olivine because the diffusivity of Ni in silicate liquid is higher than that of olivine, and this can result in anomalously high apparent $D_{Ni}^{ol/liq}$ relative to equilibrium values in what otherwise appear to be equilibrated experiments. To overcome this problem, Hart & Davis (1978) added additional Ni to their bulk starting materials and showed that their experiments were run long enough for the olivine–liquid loop (or capsule) system to reach equilibrium. The same approach (doping the bulk with significant amounts of Ni) is not readily applicable to high-pressure experiments because (1) platinum–graphite double capsule experiments have a much higher platinum to sample ratio (i.e. extremely large quantities of Ni would need to be added to the starting material to saturate the platinum with Ni) and (2) the ultimate sink of Ni in the graphite-only capsule experiments is at present unknown. As mentioned above, analyses of sintered olivines adjacent to the graphite or Re in our high-pressure experiments showed that our experiments did experience Ni loss immediately adjacent to the capsule wall while at high temperature; thus, we paid particular attention to the results of mass-balance calculations to gauge if our experimental setup successfully minimized Ni loss from melt pools in the central region of the capsules and their coexisting olivines.

The phase proportions in our experiments were determined using the non-linear approach of Albarède & Provost (1977), but the variable amount of interaction between melt and olivine from one experiment to the next requires an atypical approach to the mass-balance calculations. We allowed the starting bulk composition to vary as a linear mixture of our homogenized Juan de Fuca basalt glass and powdered Kilbourne Hole olivine starting materials (Table 1). In the calculations, the bulk NiO for each experiment was allowed to vary independently of the NiO concentration predicted by the mass fractions of starting basaltic glass and starting olivine required to mass balance the compositions of the final liquid and its equilibrium olivine for all other elements. For a given experiment, the difference between these two NiO concentrations gives an estimate of nickel loss for that run. In the 1 atm experiments, bulk Na_2O was also allowed to vary. Additional details are given in the Supplementary Material. Results of the mass-balance calculation including phase proportions of glass, olivine, and pyroxene, per cent change in Ni (and Na, where appropriate), and a goodness-of-fit value, Q, are given in Table 2. All experiments have mass-balance solutions acceptable at the 95% confidence level (Press *et al.*, 1992), suggesting that variations in liquid composition are well explained by the presence of the observed phases listed in Tables 2 and 3.

The calculated change in bulk NiO is listed for the forward experiments in Table 2 and indicates that our experimental design was successful in conserving NiO within the interior of the charge—changes range from −12 to +6% relative (where a negative number indicates a decrease of bulk NiO). This suggests that, although the outer ~100 μm rind of olivine closest to the graphite capsule lost Ni, our experimental setup was successful at minimizing the interaction of the central melt pool with the outer zone of olivine or the graphite (note that exploratory experiments without a sintered olivine inner 'capsule' run under similar pressure–temperature conditions and for similar times lost over 50% of their bulk NiO). For the reversal experiments, the mass-balance calculations suggest a gain of up to 49% NiO. These results are a numerical artifact of our use of near-liquid olivines for mass balance; these crystals gained significant NiO from the Ni-enriched starting glass and are zoned in nickel (the initial glass used in the reversal experiments has ~1 wt % NiO) and thus yield a solution to the mass-balance equations that requires a significant amount of additional NiO. In other words, although the rim olivine compositions yield an accurate $D_{Ni}^{ol/liq}$, the rim NiO concentrations do not reflect an accurate average NiO content of the reacted mass of olivine and it is for this reason that we do not report changes in bulk NiO for the reversal experiments.

Attainment of equilibrium

To demonstrate that our experiments approached equilibrium with respect to $D_{Ni}^{ol/liq}$, we conducted both time series and reversal experiments. Time invariance is a necessary, though insufficient, condition for establishing equilibrium. We conducted a time series at 1·0 GPa and 1450°C, running experiments for 6, 12, and 18 h. The partition coefficients from these experiments, shown in Fig. 1a as the three open circles at ~1450°C, range from 4·31 to 4·66 and overlap at 1σ, suggesting that $D_{Ni}^{ol/liq}$ does not change appreciably for these run durations. As described above, we also performed reversal experiments. In a forward experiment (open circles and filled square in Fig. 1a), the starting glass chip had very low NiO (below the microprobe detection limit of 0·03 wt %); that is, at the beginning of a forward experiment, the initial apparent $D_{Ni}^{ol/liq}$ of the experiment was very high (≫5); over the course of the experiment, there is a net transfer of NiO from the olivine into the liquid so that, by the end of the run, the glass has 0·07–0·10 wt % NiO. In a reversal experiment (open triangles in Fig. 1a), the initial glass has ~1 wt % NiO, making the initial apparent $D_{Ni}^{ol/liq} \sim 0{\cdot}4$, much lower than the equilibrium value; NiO moves from the melt into the olivine during the experiment, and the equilibrated glass has 0·11–0·42 wt % NiO (i.e. it has lost considerable NiO to the adjacent olivine). We conducted a total of five reversals at four pressures (1 atm, 1·0, 2·0 and 3·0 GPa); in all cases the reversal experiments yield $D_{Ni}^{ol/liq}$ values that overlap at 1σ with all of the forward experiments run at the same conditions. This, along with the 1·0 GPa time series, strongly suggests that the $D_{Ni}^{ol/liq}$ values reported here represent equilibrium values. Additionally, the Re-capsule experiment (Run 9) yields a $D_{Ni}^{ol/liq}$ indistinguishable from that of a platinum–graphite experiment (Run 10) conducted at the same pressure and temperature ($D_{Ni}^{ol/liq}$ values are $4{\cdot}38 \pm 0{\cdot}15$ and $4{\cdot}35 \pm 0{\cdot}17$, respectively; errors are 1σ, propagated from reported values in Table 3), suggesting that our results are also independent of capsule material.

Figure 1a shows $D_{Ni}^{ol/liq}$ values from all of our experiments as a function of temperature. Overall, Fig. 1a shows that measured $D_{Ni}^{ol/liq}$ in this study decreases with increasing temperature (and pressure, as the two are coupled in our experiments) from 5·0 at 1400°C (1 atm) to 3·8 at 1550°C (3 GPa). Correlation of $D_{Ni}^{ol/liq}$ with either temperature or pressure is good, with $R^2 = 0{\cdot}72$. Figure 1b compares our results with model predictions of $D_{Ni}^{ol/liq}$ from the literature and illustrates that most of the available models do not accurately recover the results of our experiments: some predict smaller and some predict larger variations with temperature (and pressure) than our results, and those that do not include a pressure or temperature term obviously predict none at all. In the following

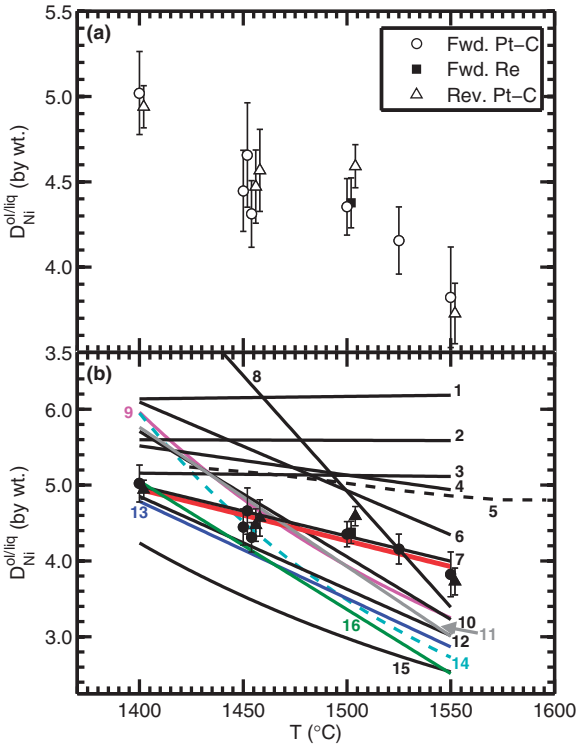

Fig. 1. $D_{Ni}^{ol/liq}$ as a function of temperature. (a) Experiments from this study. Error bars are one standard deviation of the calculated partition coefficient based on the uncertainties in average NiO contents of the glass and olivine. For clarity, we offset points by as much as 10° from the actual run temperature (i.e. all experiments plotting close to 1450°C were conducted at 1450°C). Open circles represent forward experiments, and open triangles represent reversal experiments performed in Pt–graphite double capsules. The filled square represents a Re-capsule experiment. (b) Predictions, based on literature models, for data from our experiments, which are also shown along with a linear least-squares regression fit to our data assuming that $D_{Ni}^{ol/liq}$ is a function only of temperature (red line). Symbol shapes for our data are as in panel (a). Each literature line was constructed by first calculating $D_{Ni}^{ol/liq}$ for each experiment according to the authors' model using the phase compositions given in Table 3. The resulting set of points for each expression, excepting the one labeled 'MELTS', was then fitted to a line using an unweighted least-squares analysis. 1, Hart & Davis (1978) expression assuming $D_{Ni}^{ol/liq}$ to be a function of MgO^{liq}; 2, equation (4) from Kinzler *et al.* (1990); 3, Beattie *et al.* (1991); 4, Colson *et al.* (1988); 5, MELTS calculations were performed by taking run 25, 1 atm, glass composition and varying temperature at each pressure (1 atm–3·0 GPa in 0·5 GPa increments) until a small amount of olivine crystallized; straight lines connect calculation points; 6, equation (2c) from Putirka *et al.* (2011); 7, equation (K4) using dataset 4 from Leeman & Lindstrom (1978); 8, expression from Agee & Walker (1990) assuming that $D_{Ni}^{ol/liq}$ depends on temperature and MgO^{liq}; 9, Hart & Davis (1978) assuming $D_{Ni}^{ol/liq}$ to be a function of T; 10, equation (2b) from Putirka *et al.* (2011); 11, Agee & Walker (1990) assuming that $D_{Ni}^{ol/liq}$ depends on temperature and SiO_2^{liq}; 12, equation (2a) from Putirka *et al.* (2011); 13, Li & Ripley (2010); 14, Kelemen *et al.* (1998); 15, Arndt (1977); 16, fits to equation (K3) using dataset 4 from Leeman & Lindstrom (1978).

sections, we explore the relative contributions of temperature, pressure, and phase composition to the observed variations in $D_{Ni}^{ol/liq}$ and compare our results with those from the literature.

DISCUSSION

Possible contributions of melt compositional variations in our experiments to the observed temperature and pressure dependence of $D_{Ni}^{ol/liq}$

The key feature of our experimental results is that, for liquids of approximately constant composition (especially with respect to MgO content), the Ni partition coefficient decreases with increasing temperature and pressure, from 5·0 at 1400°C (1 atm) to 3·8 at 1550°C (3 GPa). However, over this pressure–temperature range melt compositions are not strictly constant; for example, SiO_2 concentrations decrease and incompatible minor element abundances (e.g. TiO_2, K_2O, and P_2O_5) increase with increasing pressure above 2·0 GPa, resulting in statistically significant correlations between the SiO_2, K_2O, and P_2O_5 contents of the liquids and $D_{Ni}^{ol/liq}$. Here, we consider the extent to which these changes in liquid composition might contribute to the observed change in $D_{Ni}^{ol/liq}$.

(1) Melt composition varies in our experiments owing to crystallization of pyroxene in the higher-pressure runs and variable degrees of interaction between the starting glass and surrounding olivine. However, the Spearman rank–order correlation coefficient (r_s) between $D_{Ni}^{ol/liq}$ and the MgO content of the liquid (in wt %), a variable widely used to describe variations in $D_{Ni}^{ol/liq}$ (e.g. Hart & Davis, 1978; Kinzler *et al.*, 1990), is −0·05, a statistically insignificant correlation (the confidence level is only ∼14%). For example, glasses in Runs 25 (1 atm) and 30 (3·0 GPa) have essentially identical MgO contents (18·1 and 18·3 wt %) and olivine Mg# values (90·2 and 89·7); the models of Hart & Davis (1978) and Kinzler *et al.* (1990) predict $D_{Ni}^{ol/liq}$ values for these two experiments that differ by only 0·1 (or ∼2%), whereas the observed difference is 1·2 (or ∼24%). This suggests that in our experiments another parameter (or combination of parameters) is affecting $D_{Ni}^{ol/liq}$.

(2) Glasses from the 1·0 GPa experiments show a range in SiO_2 contents (48·9–50·2 wt %) over a narrow range of MgO contents (17·4–17·7 wt %; see discussion above), yet $D_{Ni}^{ol/liq}$ values from these experiments are all within 1σ of each other.

(3) As mentioned above, pyroxene crystallization resulted in higher concentrations of incompatible elements in melts from the highest-pressure experiments (Runs 30 and 33R) than in lower-pressure experiments. However, the absolute increases for these incompatible elements are small (<0·6 wt % for TiO_2 and <0·08 wt % for K_2O and P_2O_5), making it unlikely that they are responsible for the large changes of $D_{Ni}^{ol/liq}$ measured in our experiments.

(4) As noted above, for our entire dataset, there is a statistically significant positive correlation between SiO_2 and $D_{Ni}^{ol/liq}$ ($r_s = 0·49$, significant at the 91% confidence level). However, this correlation is being driven largely by the relatively low silica contents in the 2·5 and 3 GPa experimental

glasses that crystallized more than trace amounts of pyroxene. Liquid silica contents and $D_{Ni}^{ol/liq}$ values from runs between 1 atm and 2 GPa are uncorrelated at the 1σ level, yet over this same pressure interval, T and $D_{Ni}^{ol/liq}$ are still negatively correlated at the ~94% confidence level. In the Supplementary Material, we add simplified regular-solution-like terms to our partitioning models (introduced below) to formulate expressions that include the effects of MgO and SiO_2 in the melt on $D_{Ni}^{ol/liq}$. We use these expressions to argue that the small variations of the MgO and SiO_2 contents of the liquids of our experiments are expected to have a much smaller effect on $D_{Ni}^{ol/liq}$ (~5%) than pressure and temperature (~24%).

From these considerations and the analysis included in the Supplementary Material, we find no evidence to suggest that differences in melt composition between experiments contribute significantly to the observed systematic decrease in $D_{Ni}^{ol/liq}$, but rather that temperature and/or pressure are the dominant drivers of the observed variations in $D_{Ni}^{ol/liq}$.

Comparing our data with previous partitioning expressions

As emphasized in the Introduction, knowing how temperature, pressure, and melt and olivine composition affect $D_{Ni}^{ol/liq}$ is crucial for petrogenetic modeling. Figure 1b compares our experimental $D_{Ni}^{ol/liq}$ values with various published models used for calculating $D_{Ni}^{ol/liq}$. Not surprisingly, those models that attribute variations in $D_{Ni}^{ol/liq}$ to olivine and liquid composition alone (Hart & Davis, 1978; Kinzler *et al.*, 1990; Beattie *et al.*, 1991) predict essentially no change in $D_{Ni}^{ol/liq}$ for our experiments because the melt and olivine compositions in our experiments are essentially constant. On the other hand, models that attribute changes in $D_{Ni}^{ol/liq}$ solely to temperature (Arndt, 1977; Hart & Davis, 1978; Kelemen *et al.*, 1998) overpredict the temperature dependence (i.e. the slope of the model $D_{Ni}^{ol/liq}$ vs temperature trend is more negative than that shown by our data). As we discuss below, a simple thermodynamic analysis suggests that both composition and temperature probably affect $D_{Ni}^{ol/liq}$. Thus, it is not surprising that attributing changes to one or the other variable alone leads to models that underpredict or overpredict the actual variation in $D_{Ni}^{ol/liq}$ in certain circumstances. The thermodynamically inspired empirical expressions of Li & Ripley (2010), equation (K3) from Leeman & Lindstrom (1978), and all equations from Putirka *et al.* (2011) also overpredict the dependence of $D_{Ni}^{ol/liq}$ on temperature observed in our experiments. The TEX model of Colson *et al.* (1988) and the MELTS thermodynamic model (Ghiorso & Sack, 1995; Smith & Asimow, 2005) come relatively close to reproducing the temperature dependence of our data, although these models predict $D_{Ni}^{ol/liq}$ values that are systematically high relative to our data (by ~10% at 1400°C and ~30% at 1550°C). Equation (K4) (fitted to their dataset number 4) from Leeman & Lindstrom (1978) (labeled 7 in Fig. 1b) reproduces the temperature dependence of our data remarkably well. In the following sections, we develop two simple thermodynamic treatments based on ideal exchange and formation reactions that successfully describe both our data and those from the literature.

Fitting $D_{Ni}^{ol/liq}$ using an ideal exchange reaction

Data from this work

We first fit our $D_{Ni}^{ol/liq}$ data to a Ni–Mg exchange reaction (e.g. Hart & Davis, 1978; Leeman & Lindstrom, 1978; Kinzler *et al.*, 1990):

$$MgSi_{0.5}O_2^{ol} + NiO^{liq} \leftrightarrow NiSi_{0.5}O_2^{ol} + MgO^{liq}. \quad (1)$$

Writing the equilibrium constant for reaction (1) yields

$$\Delta_{r(1)}G^{\circ}_{T,P} = -RT\ln\left(\frac{X^{ol}_{NiSi_{0.5}O_2}X^{liq}_{MgO}}{X^{ol}_{MgSi_{0.5}O_2}X^{liq}_{NiO}} \times \frac{\gamma^{ol}_{NiSi_{0.5}O_2}\gamma^{liq}_{MgO}}{\gamma^{ol}_{MgSi_{0.5}O_2}\gamma^{liq}_{NiO}}\right) \quad (2)$$

Where $\Delta_{r(1)}G^{\circ}_{T,P}$ is the standard-state Gibbs free energy of reaction (1) at a given pressure and temperature, and X_i^{φ} and γ_i^{φ} are the mole fraction and activity coefficient of the ith component in phase φ (the selected molar components and an example calculation is included in the Supplementary Material). The explicit dependence of $\Delta_{r(1)}G^{\circ}_{T,P}$ on temperature and pressure is

$$\Delta_{r(1)}G^{\circ}_{T,P} = \Delta_{r(1)}H^{\circ}_{T_{ref},P_{ref}} + \int_{T_{ref}}^{T}\Delta_{r(1)}C_p^{\circ}\,dT - T\left[\int_{T_{ref}}^{T}\left(\frac{\Delta_{r(1)}C_p^{\circ}}{T}\right)dT + \Delta_{r(1)}S^{\circ}_{T_{ref},P_{ref}}\right] + \int_{P_{ref}}^{P}\Delta_{r(1)}V\,dP \quad (3)$$

Where $\Delta_{r(1)}H^{\circ}_{T_{ref},P_{ref}}$ and $\Delta_{r(1)}S^{\circ}_{T_{ref},P_{ref}}$ are the standard state enthalpy and entropy changes of reaction (1) at the reference pressure, P_{ref}, and temperature, T_{ref}; $\Delta_{r(1)}C_p^{\circ}$ is the temperature-dependent, isobaric change in heat capacity of the reaction at P_{ref}; and $\Delta_{r(1)}V$ is the temperature- and pressure-dependent volume change of the reaction at temperature and pressure. If we define the molar partition coefficient as $D_{Ni}^{molar} = X^{ol}_{NiSi_{0.5}O_2}/X^{liq}_{NiO}$ and combine equations (2) and (3), we obtain

$$-\frac{\Delta_{r(1)}H^{\circ}_{T_{ref},P_{ref}}}{RT} + \frac{\Delta_{r(1)}S^{\circ}_{T_{ref},P_{ref}}}{R} = \ln(D_{Ni}^{molar}) + \ln\left(\frac{X^{liq}_{MgO}}{X^{ol}_{MgSi_{0.5}O_2}}\right) + \ln\left(\frac{\gamma^{ol}_{NiSi_{0.5}O_2}\gamma^{liq}_{MgO}}{\gamma^{ol}_{MgSi_{0.5}O_2}\gamma^{liq}_{NiO}}\right) + \frac{\int_{T_{ref}}^{T}\Delta_{r(1)}C_p^{\circ}\,dT}{RT} - \frac{\int_{T_{ref}}^{T}(\Delta_{r(1)}C_p^{\circ}/T)\,dT}{R} + \frac{\int_{P_{ref}}^{P}\Delta_{r(1)}V\,dP}{RT}. \quad (4)$$

Equation (4) is general, but it is usually simplified by making various plausible and/or expedient assumptions. In particular, for exchange reactions such as reaction (1), it is usually assumed that $\Delta_{r(1)}C_p^\circ$ and $\Delta_{r(1)}V$ are small enough to be negligible. However, sufficient thermodynamic data are available to explicitly test this set of assumptions. We used heat capacities for olivine from Berman (1988) and Hirschmann (1991), and heat capacities for liquids from Chase (1998). To calculate the standard state volume change of reaction (1), we used expressions for the volume of forsterite from Berman & Aranovich (1996). Following Hirschmann (1991), we fitted the Ni-olivine data of Vokurka & Rieder (1987) to obtain the reference volume and thermal expansion coefficients and took the compressibility measurements from Bass *et al.* (1984). Data are not available for volumes of liquid NiO and MgO. We therefore estimated standard state liquid volumes through stoichiometric olivine liquids (e.g. $MgSi_{0.5}O_2$) using a third-order Birch–Murnaghan equation of state with a K' of five, assuming ideal volumes of mixing of the oxide components. It should be noted that if the mixing volumes for NiO–$Si_{0.5}O$ and MgO–$Si_{0.5}O$ are ideal (or if the excess terms are equivalent) the difference in volume between $MgSi_{0.5}O_2$ and $NiSi_{0.5}O_2$ will be the same as the difference between MgO^{liq} and NiO^{liq}. For forsterite liquid, the reference volume and compressibility were taken from Ai & Lange (2008) and the thermal expansivity from Ghiorso (2004). Because of the absence of data on Ni-olivine liquid, we followed Hirschmann & Ghiorso (1994) and used data for fayalite liquid; specifically, compressibility from Chen *et al.* (2002) and thermal expansivity from Ghiorso (2004). The reference volume for Ni-olivine liquid was set such that the volume change on melting [defined as $(V_{melt} - V_{solid})/V_{solid}$ at 1 bar] at the melting temperature was 10%, similar to that of fayalite (9·9%) and forsterite (9·2%). If we choose a reference temperature of 1662 K, to minimize nonzero contributions for applications to literature data described below, and use the data and approximations as described above, the calculated $\Delta_{r(1)}C_p^\circ$ and $\Delta_{r(1)}V$ terms in equation (4) are small enough to be negligible: over the temperature and pressure range of our experiments, the sum of the final three terms (those involving $\Delta_{r(1)}C_p^\circ$ and $\Delta_{r(1)}V$) of equation (4) (-1×10^{-4} to 5×10^{-3}) is 1–2 orders of magnitude smaller than the errors on the sum of the compositional terms [$\ln D_{Ni}^{molar} + \ln(X_{MgO}^{liq}/X_{MgSi_{0.5}O_2}^{ol})$] ($3\times10^{-2}$ to 9×10^{-2}). We conclude that for reaction (1) we can safely approximate $\Delta_{r(1)}C_p^\circ$ and $\Delta_{r(1)}V$ as zero, which means that we expect there to be no significant pressure effect on $D_{Ni}^{ol/liq}$ (or D_{Ni}^{molar}) for our experiments if we model the results using the exchange reaction (1); this is a critical point because it suggests that although temperature and pressure covaried in our experiments, variations in $D_{Ni}^{ol/liq}$ can be regarded as essentially due to variations in temperature.

A useful starting point for understanding compositional effects on D_{Ni}^{molar} is to assume that melt and olivine are ideal solutions so that the activity coefficients are all unity [or, equivalently, that they are not unity but cancel in equation (4)]. Equation (4) then simplifies to

$$-\frac{\Delta_{r(1)}H^\circ_{T_{ref},P_{ref}}}{RT}+\frac{\Delta_{r(1)}S^\circ_{T_{ref},P_{ref}}}{R}=\ln(D_{Ni}^{molar})+\ln\left(\frac{X_{MgO}^{liq}}{X_{MgSi_{0.5}O_2}^{ol}}\right). \quad (5)$$

Terms on the right-hand side of equation (5) can all be obtained from phase compositions in an experiment, so $\Delta_{r(1)}H^\circ_{T_{ref},P_{ref}}$ and $\Delta_{r(1)}S^\circ_{T_{ref},P_{ref}}$ are unknowns but, based on our stated assumptions, they are independent of pressure and temperature and can be readily solved for with a series of experiments covering a range of temperatures.

Equation (5) is a natural starting point for fitting experimentally determined olivine–liquid Ni partitioning data (e.g. Hart & Davis, 1978; Leeman & Lindstrom, 1978; Kinzler *et al.*, 1990), but even in this simplified version, D_{Ni}^{molar} depends independently on temperature and melt and olivine composition; for example, D_{Ni}^{molar} will vary with temperature (provided $\Delta_{r(1)}H^\circ_{T_{ref},P_{ref}} \neq 0$) and will decrease with increasing MgO content of the melt and decreasing forsterite content of the olivine (e.g. Hart & Davis, 1978; Kinzler *et al.*, 1990). As emphasized in the Introduction, this is an important point: although these three variables are often strongly correlated in igneous processes (and therefore may not always appear to be independently variable), there are circumstances in which they can vary independently, and separation of their effects as in equation (5) becomes critical. An example of such a situation is evaluated below in connection with Ni-rich olivines observed in Hawaii. It should be noted that the form of equation (5) is the same if the phases are Henrian, but then the constant on the left-hand side of the equation, $\Delta_{r(1)}S^\circ_{T_{ref},P_{ref}}/R$, would also include a term containing the activity coefficients.

By design, phases from our experiments vary little in composition (particularly with respect to the MgO content of the melt and the forsterite content of the coexisting olivine) and thus they provide constraints on $\Delta_{r(1)}H^\circ_{T_{ref},P_{ref}}$ and $\Delta_{r(1)}S^\circ_{T_{ref},P_{ref}}$, assuming as we have done in deriving equation (5) that the activity coefficients are not strong functions of temperature (e.g. Holzheid *et al.*, 1997) or pressure, and that the resulting ratio of activity coefficients is small. We fitted our data to equation (5) using a robust algorithm (iterative, bisquare-weighted, least-squares fit, implemented in MATLAB); the resulting values of $-\Delta_{r(1)}H^\circ_{T_{ref},P_{ref}}/R$ and $\Delta_{r(1)}S^\circ_{T_{ref},P_{ref}}/R$ are 4375 K and −2·023, respectively. The fit is shown graphically in Fig. 2 (continuous black line), and describes well the observed variation in D_{Ni}^{molar} as a function of temperature from our experiments (filled black symbols); that is, the average error associated with the fit is ∼4%, which is comparable with the ∼5% uncertainty associated with each D_{Ni}^{molar}

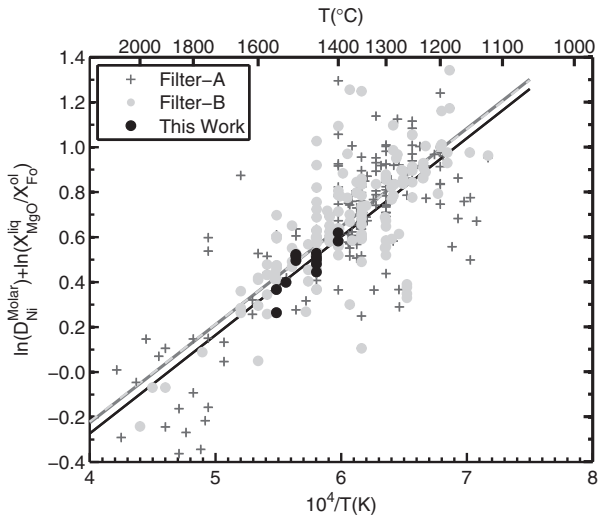

Fig. 2. $\ln(D_{Ni}^{molar}) + \ln(X_{MgO}^{liq}/X_{Fo}^{ol})$ as a function of $10^4/T$ (K) [compare equation (5) where $X_{Fo}^{ol} = X_{MgSi_{0\cdot5}O_2}^{ol}$]. Each point represents the result for a single experiment and lines are robust fits to a given dataset. Experiments passing Filter-A only are shown as dark gray crosses and a robust fit is shown as a continuous dark gray line. Data passing Filter-B are shown as light gray filled circles (experiments that pass the Filter-B dataset are included in the Filter-A fits but are not plotted separately) and a robust fit is shown as a light gray dashed line. Data from this work are plotted as filled black circles with the corresponding robust fit shown by a continuous black line.

value. A comparison and short discussion of our fitted values of $-\Delta_{r(1)}H^{\circ}_{T_{ref},P_{ref}}/R$ and $\Delta_{r(1)}S^{\circ}_{T_{ref},P_{ref}}/R$ and those calculated from tabulated thermodynamic data are included in the Supplementary Material.

Data from the literature

Our experiments were designed to isolate the effects of phase composition from those of temperature and pressure on $D_{Ni}^{ol/liq}$ by holding phase compositions constant and varying temperature and pressure. As we showed above, the effect of pressure can be neglected if the exchange reaction (1) is used to describe Ni partitioning. Because the phase compositions in our experiments are essentially constant, our experiments are poorly posed to evaluate the approximation that the activity coefficient ratio in equation (4) is unity or can be treated as a constant and subsequently incorporated into the $\Delta_{r(1)}S^{\circ}_{T_{ref},P_{ref}}/R$ term. To test this assumption, we utilized the extensive experimental literature data on olivine–liquid Ni partitioning. These data span a wide range of melt and olivine compositions and they can also be fitted to equation (5). Comparing the temperature dependence derived from a fit to the literature data—which span a wide compositional range—to the well-constrained temperature dependence from our experiments will allow us to further assess the validity of the simplifying assumptions we made for equation (5).

We constructed two datasets from the literature for the purpose of exploring relationships between melt composition and $D_{Ni}^{ol/liq}$. In the first of these, we accepted our 13 experiments plus 312 experiments from the literature for which both glass and olivine analytical totals fell in the range of 98·5–101·5% (the full database has 434 experiments; all database references are listed in the Supplementary Material). In this and all further datasets we also excluded experiments from Leeman (1974) with less than 0·05 wt % NiO in the liquid (even if they passed the oxide totals criteria) because, in our initial fits, these experiments exhibited particularly large residuals. It is likely that the low NiO content of these liquids, coupled with the analytical capabilities of early electron microprobes, resulted in large uncertainties in the $D_{Ni}^{ol/liq}$ values. We refer to this dataset, filtered primarily by analytical totals, as Filter-A. Although some olivines have high Ni contents (up to 31·6 wt % NiO), we ignore possible non-Henrian behavior [see Beattie (1993*b*) for a discussion], noting that the resulting fits do not change significantly if we exclude those experiments in which olivines have more than 6 wt % NiO.

In addition to the Filter-A dataset, we also developed a more restrictive dataset, Filter-B. As we emphasized above, experiments that experience a net loss of Ni may yield anomalously high $D_{Ni}^{ol/liq}$ values even though they appear to be in equilibrium (Hart & Davis, 1978). In an attempt to filter out such non-equilibrium $D_{Ni}^{ol/liq}$ values, we mass balanced those experiments in the Filter-A dataset for which all coexisting phases had been analyzed (274 out of 312). Of the 274 runs, 197 yielded solutions acceptable at the 95% confidence level (details of our mass-balance approach are given in the Supplementary Material). As with the experiments from this study, bulk NiO was treated as a variable when mass balancing the literature experiments thus providing a quantitative measure of the amount of Ni lost or gained from these runs. In only 56% of the 197 experiments did bulk NiO concentrations change by less than 5%; the largest changes were −91 and +96%, respectively. However, a relatively large change in bulk NiO does not necessarily mean that the experiment in question should be rejected. For example, the experiments of Hart & Davis (1978) were designed to saturate the Pt loop or capsule with Ni during the run and thus their starting compositions were enriched in NiO. Despite losing large amounts of NiO to the sample container, Hart & Davis (1978) showed, via time-series experiments, that their run times were sufficient to approach steady-state $D_{Ni}^{ol/liq}$ values. In contrast, the mass-balance calculations indicate that experiments run on pure Ni-wire loops (e.g. Snyder & Carmichael, 1992) gained a relatively large amount of bulk NiO. Our Filter-B dataset contains those experiments that were successfully mass balanced and either show less than 65% relative change in bulk NiO or explicitly demonstrated an approach to equilibrium despite larger amounts of Ni loss [experiments of Leeman (1974)

run above 1300°C and >144 h; Arndt, 1977; Hart & Davis, 1978; experiments of Takahashi (1978) run above 1320°C and >15 h; Campbell *et al.*, 1979; Nabelek, 1980; Drake & Holloway, 1981; Seifert *et al.*, 1988; Kinzler *et al.*, 1990; Snyder & Carmichael, 1992; Mysen, 2006, 2007]. The Supplementary Material contains additional details on the construction of the Filter-B dataset. Based on these criteria, 168 experiments (including the 13 runs from this study) are included in the Filter-B dataset.

In contrast to the new work presented here, the Filter-A and Filter-B datasets span a wide compositional range: SiO_2 and MgO in the liquid range of 34–70 and 3–40 wt % for the Filter-A dataset, and the Filter-B dataset spans similar ranges, 40–69 wt % SiO_2 and 4–38 wt % MgO; the olivines from both datasets have Mg# values that range from 36 to 100. The experiments from the literature also span a significantly larger pressure–temperature range than our experiments; the Filter-B dataset contains experiments performed at temperatures up to 2000°C and pressures as high as 10 GPa, requiring us to check our earlier assumption that $\Delta_{r(1)}C_p^\circ$ and $\Delta_{r(1)}V$ are small enough to be approximated as zero. At these high temperatures and pressures our earlier approximation that $\Delta_{r(1)}C_p^\circ$ and $\Delta_{r(1)}V$ are zero remains valid. The magnitude of the sum of the heat capacity and volume terms in equation (4) can be as large as 0·23, greater than the compositional error of our experiments (~0·1); however, including the volume and heat capacity terms in the robust-fitting algorithm makes no statistical difference in the resulting fits. This result is not definitive, as the highest pressure–temperature experiments were conducted at pressures well above the applicable upper limit of our liquid equation of state (~4 GPa, Ghiorso *et al.*, 2002), and at these extreme temperatures we have decreasing confidence in the validity of the assumptions used to support ignoring the heat capacity terms in reaction (1).

The Filter-A and Filter-B datasets were fitted to equation (5) using the same approach as we used to fit our experimental results (see previous section). The fits are shown graphically in Fig. 2 and listed in Table 4; also listed in Table 4 are the average per cent errors between the predicted and measured $D_{Ni}^{ol/liq}$ values. Figure 2 shows that the fit to our experimental data is nearly parallel and only slightly offset from the lines based on the Filter-A and Filter-B datasets (the latter two lines plot on top of one another in Fig. 2). Moreover, for all three fits, values for $-\Delta_{r(1)}H^\circ_{T_{ref},P_{ref}}/R$ and $\Delta_{r(1)}S^\circ_{T_{ref},P_{ref}}/R$ overlap at one standard error. Although it is not readily apparent in Fig. 2, it should be noted that the Filter-A data are considerably more scattered than the Filter-B data, leading to a mean residual that is ~2·5 times larger than for the Filter-B dataset. A corollary of the increased scatter is that the mean per cent error on $D_{Ni}^{ol/liq}$ is somewhat larger for the Filter-A dataset (14% for Filter-A vs 12% for Filter-B). Owing to the similarity of the fit parameters, however, both best-fit equations for literature data predict $D_{Ni}^{ol/liq}$ for our experiments equally well: in both cases, the average error on $D_{Ni}^{ol/liq}$ for our experiments is 6·0%, only slightly larger than the fit to our data alone (3·9%). Although both the Filter-A and Filter-B datasets yield fit parameters to equation (5) that are similar to those derived using our experiments alone, our experiments are critical to interpreting the larger literature database because they combine the unique features of a wide temperature range with limited compositional variability (i.e. our results are independent of approximations regarding the effect of composition on $D_{Ni}^{ol/liq}$), unambiguously allowing us to characterize the temperature dependence of $D_{Ni}^{ol/liq}$.

Fitting $D_{Ni}^{ol/liq}$ using an ideal formation reaction

In addition to working with the exchange reaction (1), we also fitted our data together with those of the literature to a Ni-olivine formation reaction (e.g. Leeman & Lindstrom, 1978; Kinzler *et al.*, 1990):

$$Si_{0.5}O^{liq} + NiO^{liq} \leftrightarrow NiSi_{0.5}O_2^{ol}. \quad (6)$$

Writing an equilibrium constant expression for this reaction and defining the molar partition coefficient as above, and rearranging, yields

$$\begin{aligned} -\frac{\Delta_{r(6)}H^\circ_{T_{ref},P_{ref}}}{RT} + \frac{\Delta_{r(6)}S^\circ_{T_{ref},P_{ref}}}{R} &= \ln(D_{Ni}^{molar}) \\ &+ \ln\left(\frac{1}{X_{Si_{0.5}O}^{liq}}\right) + \ln\left(\frac{\gamma_{NiSi_{0.5}O_2}^{ol}}{\gamma_{NiO}^{liq}\gamma_{Si_{0.5}O}^{liq}}\right) \\ &+ \frac{\int_{P_{ref}}^{P}\Delta_{r(6)}V\,dP}{RT} + \frac{\int_{T_{ref}}^{T}\Delta_{r(6)}C_p^\circ\,dT}{RT} - \frac{\int_{T_{ref}}^{T}(\Delta_{r(6)}C_p^\circ/T)\,dT}{R}. \end{aligned} \quad (7)$$

Unlike the exchange reaction [equations (1)–(5)], for which $\Delta_r C_p^\circ$ and $\Delta_r V$ are sufficiently small that they can be neglected, in the Ni-olivine formation reaction (6), these two variables are of sufficient magnitude that they must be explicitly included [however, it should be noted that by choosing T_{ref} within the temperature range of interest, one can minimize the significance of the two $\Delta_{r(6)}C_p^\circ$ terms in (7)]. For our experiments, with a reference temperature of 1662 K, the two $\Delta_{r(6)}C_p^\circ$ terms are small, with absolute values up to 0·06% of $[\ln(D_{Ni}^{molar}) + \ln(1/X_{Si_{0.5}O}^{liq})]$; whereas the volume term, $(\int_{P_{ref}}^{P}\Delta_{r(6)}VdP)/RT$ (P_{ref} = 1 bar), is significant, with absolute values ranging from zero to 9% of $[\ln(D_{Ni}^{molar}) + \ln(1/X_{Si_{0.5}O}^{liq})]$. Values are similar for the larger Filter-B dataset, the experiments of which span a larger range of temperatures and pressures; absolute value of heat capacity and volume terms are as high as 1% and

Table 4: Fit parameters

Reaction fit	Dataset fit	$-\Delta_r H^\circ_{T_{ref},P_{ref}}/R$ (K)[1]	$-\Delta_r S^\circ_{T_{ref},P_{ref}}/R$	Mean per cent errors[2] when predicting $D_{Ni}^{ol/liq}$ from		
				Filter-A	Filter-B	This work only
Exch, ideal[3]	This work	4375(1050)	−2·023(602)	13·9	12·2	3·9
Exch, ideal[3]	Filter-A	4362(156)	−1·970(95)	13·9	12·0	6·0
Exch, ideal[3]	Filter-B	4338(208)	−1·956(126)	13·9	12·0	6·0
Fm, ideal[4]	Filter-A	9931(232)	−3·144(141)	18·4	17·6	8·6
Fm, ideal, $\Delta_{r(6)}C_p$, $\Delta_{r(6)}V$ [5]	This work	8795(798)	−2·620(457)	18·8	17·5	3·1
Fm, ideal, $\Delta_{r(6)}C_p$, $\Delta_{r(6)}V$ [5]	Filter-A	10 749(215)	−3·664(130)	17·5	16·0	8·2
Fm, ideal, $\Delta_{r(6)}C_p$, $\Delta_{r(6)}V$ [5]	Filter-B	11 239(255)	−3·970(154)	17·2	15·6	6·2

For each fit, we list the reaction [Exch for exchange reaction (1) and Fm for formation reaction (6)], the dataset used, and the resulting fit parameters.
[1]For all fit parameters, units are listed in parenthesis in the column header, where not unitless. Number in parenthesis is the standard error of the fit parameter in terms of the last unit cited [e.g. 4375(1050) should be read as 4375 with an estimated standard error of 1050; standard errors are estimated using the robustfit function in MATLAB].
[2]Mean per cent errors are defined as 100 times the absolute difference between the predicted and measured nickel partition coefficient divided by the measured value for each run summed over all experiments and then divided by the number of runs (n): $\sum[100 \times (|\text{predicted } D_{Ni}^{ol/liq} - \text{measured } D_{Ni}^{ol/liq}|)/\text{measured } D_{Ni}^{ol/liq}]/n$.
[3]Equation (5).
[4]Equation (7), assuming ideality and that $\Delta_{r(6)}C_p$ and $\Delta_{r(6)}V$ are both zero.
[5]Equation (7), assuming ideality and calculating $\Delta_{r(6)}C_p$ and $\Delta_{r(6)}V$ as described in the text.

11%, respectively, of $[\ln(D_{Ni}^{molar}) + \ln(1/X_{Si_{0.5}O}^{liq})]$. The importance of retaining $\Delta_{r(6)}C_p^\circ$ and $\Delta_{r(6)}V$ in equation (7) is shown in Fig. 3. In Fig. 3a, fits to equation (7) are shown for each of the three datasets, assuming $\Delta_{r(6)}C_p^\circ$ and $\Delta_{r(6)}V$ are zero and using measured phase compositions to determine $[\ln(D_{Ni}^{molar}) + \ln(1/X_{Si_{0.5}O}^{liq})]$. The Filter-A and Filter-B datasets yield best-fit lines with slopes very different from the one required by our data. On the other hand, if $\Delta_{r(6)}C_p^\circ$ and $\Delta_{r(6)}V$ values are instead calculated for each run, the best-fit lines are similar for all three datasets (Fig. 3b). The importance of including these terms is that in our experiments and in the data from the literature temperature and pressure are correlated; a failure to account for the large volume change of reaction (6) leads to an incorrect value for $\Delta_{r(6)}H^\circ_{T_{ref},P_{ref}}$ and then results in an apparent disagreement between our experiments and those from the literature. Furthermore, it seems likely that disagreements between the temperature dependence of $D_{Ni}^{ol/liq}$ for our experiments and predictions of equation (2b) of Putirka *et al.* (2011), equation (K3) of Leeman & Lindstrom (1978), and equation (4) of Li & Ripley (2010) (Fig. 1b), reflect the use by those researchers of a functional form similar to equation (7) without accounting for $\Delta_{r(6)}C_p^\circ$ and $\Delta_{r(6)}V$. Below we describe in more detail fits to equation (7) that take $\Delta_{r(6)}C_p^\circ$ and $\Delta_{r(6)}V$ into account.

The $\Delta_{r(6)}H^\circ_{T_{ref},P_{ref}}$ and $\Delta_{r(6)}S^\circ_{T_{ref},P_{ref}}$ values for the best-fit lines in Fig. 3b are listed in Table 4 along with each fit's mean error. We fit both Filter-A and Filter-B datasets using equation (7), assuming ideal behavior. It should be noted that, as for the exchange reaction, we assume activity coefficients that are either unity or have a constant ratio, and in the special case that the phases are Henrian, the form of equation (7) is the same but then the constant on the left-hand side of the equation would also include activity coefficient terms. Fits using the formation reaction tend to have larger average errors on $D_{Ni}^{ol/liq}$ than fits to the exchange reaction; for example, 15·6% (formation) vs 12·0% (exchange) average error on $D_{Ni}^{ol/liq}$ for the Filter-B dataset.

In addition to the fact that the mean error associated with the exchange reaction applied to the Filter-B dataset is somewhat smaller than that associated with the formation reaction (i.e. using non-zero $\Delta_{r(6)}C_p^\circ$ and $\Delta_{r(6)}V$ terms), we prefer the exchange reaction (1) for the following reasons.

(1) It is possible that the assumptions we made regarding the physical properties of the components of the reaction contribute to errors in the overall fit. Recall that the volume of NiO in the liquid is not well constrained and that, for the formation reaction (6), the inclusion of a $\Delta_{r(6)}V$ term is important for reconciling our data with those from the literature. In contrast, $\Delta_{r(1)}V$ of the exchange reaction (1) is small and any errors in the way we have treated the volume of the liquid components are much more likely to cancel.

(2) The non-zero $\Delta_{r(6)}V$ of the formation reaction (6) results in a predictive expression for $D_{Ni}^{ol/liq}$ that is a function

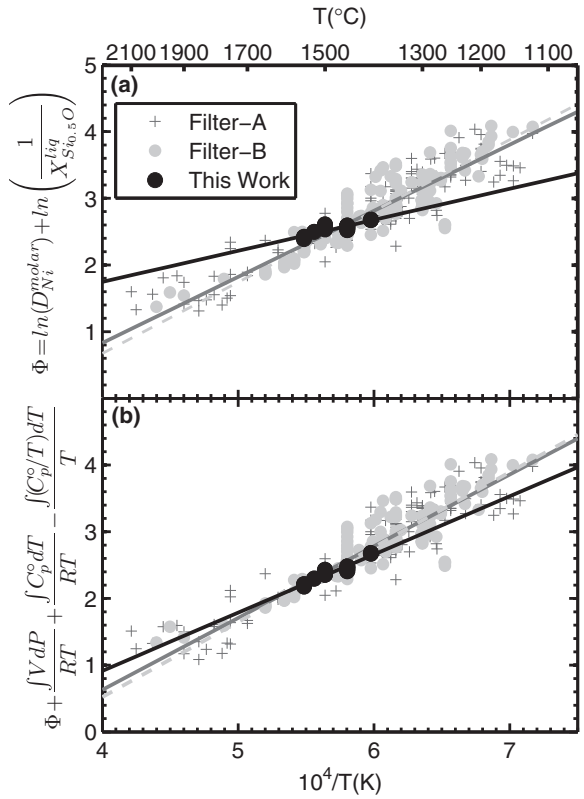

Fig. 3. Fits to the formation reaction (6) assuming ideal behavior. Fits in panel (a) assume $\Delta_{r(6)}C_p^\circ$ and $\Delta_{r(6)}V$ are zero, in which case the right-hand side of equation (7) becomes $\ln(D_{\mathrm{Ni}}^{\mathrm{molar}}) + \ln(1/X_{\mathrm{Si_{0.5}O}}^{\mathrm{liq}})$ as a function of $10^4/T$ (K); symbols are as in Fig. 2. (b)

$$\ln(D_{\mathrm{Ni}}^{\mathrm{molar}}) + \ln\left(\frac{1}{X_{\mathrm{Si_{0.5}O}}^{\mathrm{liq}}}\right) + \frac{\int_{P_{\mathrm{ref}}}^{P} \Delta_{r(6)} V \mathrm{d}P}{RT} + \frac{\int_{T_{\mathrm{ref}}}^{T} \Delta_{r(6)} C_p^\circ \mathrm{d}T}{RT} - \frac{\int_{T_{\mathrm{ref}}}^{T} (\Delta_{r(6)} C_p^\circ / T) \mathrm{d}T}{R}$$

as a function of $10^4/T$ (K) (see text for a discussion of the volumes and heat capacities used). In both panels, each point represents the result for a single experiment and lines are robust fits to a given dataset. Experiments passing Filter-A only are shown as dark gray crosses and a robust fit is shown as a continuous dark gray line. Data passing Filter-B are shown as light gray filled circles (experiments that pass the Filter-B dataset are included in the Filter-A fits but are not plotted separately) and the robust fit is shown as a dashed light gray line. Data from this work are plotted as filled black circles with the corresponding robust fit shown by a continuous black line.

of pressure. In many igneous processes, however, the pressure may not be well constrained and using the exchange reaction [equation (5) where $D_{\mathrm{Ni}}^{\mathrm{ol/liq}}$ is not dependent on pressure] may introduce less error.

(3) Because the activity coefficient term in (7) consists of Ni-olivine in the numerator and both a network-forming and network-modifying cation in the liquid in the denominator, the term is unlikely to be constant except over a very limited range of phase compositions (e.g. Ryerson, 1985). This contrasts with the activity coefficient term associated with the exchange reaction (4), where the ratios of the olivine coefficients and the network-modifying coefficients may well be approximated as a constant over a wide range of compositions (e.g. O'Neill & Berry, 2006).

Comparing Ni with other divalent cations

An in-depth discussion of the partitioning behavior of cations other than Ni between olivine and liquid is beyond the scope of this study, but it is nevertheless useful to compare Ni–Mg exchange with those of Co–Mg, Mn–Mg, and Fe–Mg. It is well known that $K_{\mathrm{D,Fe^{2+}-Mg}}$ for olivine and liquid [$K_{\mathrm{D,Fe^{2+}-Mg}} = (\mathrm{FeO/MgO})^{\mathrm{ol}}/(\mathrm{FeO/MgO})^{\mathrm{liq}}$] is relatively insensitive to temperature (e.g. Roeder & Emslie, 1970; Longhi *et al.*, 1978; Ford *et al.*, 1983; Toplis, 2005; Matzen *et al.*, 2011). Yet the key message of our experiments and of our analysis of the literature data for Ni–Mg exchange is that the equivalent parameter, $K_{\mathrm{D,Ni-Mg}} = (\mathrm{NiO/MgO})^{\mathrm{ol}}/(\mathrm{NiO/MgO})^{\mathrm{liq}}$ (or $D_{\mathrm{Ni}}^{\mathrm{ol/liq}}/D_{\mathrm{Mg}}^{\mathrm{ol/liq}}$) decreases significantly with increasing temperature (e.g. Fig. 2). That Ni–Mg exchange is qualitatively different from Fe^{2+}–Mg exchange and, indeed, from Co–Mg and Mn–Mg exchange can be illustrated using the experimental results of Takahashi (1978). We have written expressions analogous to equation (5) for Mn–Mg, Co–Mg, and Fe^{2+}–Mg exchange reactions and, in Fig. 4, we show fits to these expressions for the data of Takahashi (1978), continuous lines labeled T78. As seen in Fig. 4, the temperature dependence of the Ni–Mg exchange reaction is much larger than for any of the other three divalent cations coupled with Mg (all of which are nearly temperature independent). Fits to M^{2+}–Mg exchange for all the experiments in the Filter-B dataset, also shown in Fig. 4 (dashed lines), agree well with those of the Takahashi (1978) data, demonstrating that this is a general result and not some artifact of the Takahashi dataset.

The heat of fusion of Ni_2SiO_4 is much higher than those of Mg, Fe, or Co olivines, which is consistent with a significant difference in the temperature dependence of Ni–Mg exchange relative to other divalent cation pairs (e.g. Sugawara & Akaogi, 2003), but the underlying cause is unclear. A related issue is why should nickel be compatible in olivine in equilibrium with naturally occurring silicate melts, but incompatible in the Ni_2SiO_4–Mg_2SiO_4 binary system (e.g. Ringwood, 1956). Crystal-field stabilization energy (e.g. Burns & Fyfe, 1966) and preferential partitioning into non-equivalent olivine sites (e.g. Wood, 1974; Henderson *et al.*, 2001) are often cited as explanations for the unique behavior of Ni. Differences in Ni coordination in the melt as a function of composition undoubtedly also affect partitioning. However, available data suggest that ratios of NiO to other oxide activities, which should track large differences in coordination, are roughly constant, at least in complex melts (e.g. O'Neill & Berry, 2006). Quantitatively testing these suggestions is difficult given

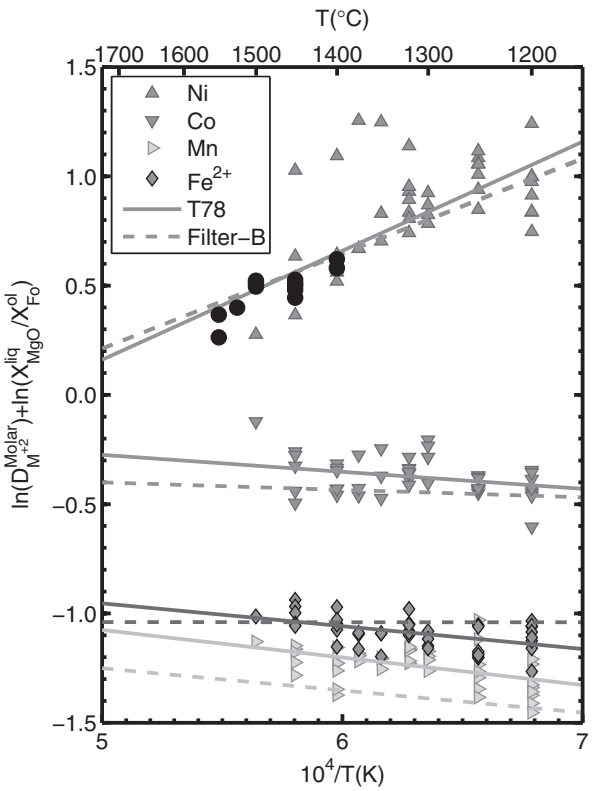

Fig. 4. M^{2+}–Mg exchange as a function of $10^4/T$ (K) for data from Takahashi (1978). Ferric iron contents were calculated for 1 atm glasses where the fO_2 or gas mixing volumes were reported and for those high-pressure experiments run in the presence of a buffer or in a graphite capsule (assuming an oxygen fugacity 0·7 log units below the CCO buffer; Médard *et al.*, 2008) using the expression of O'Neill *et al.* (2006); experiments with insufficient information to calculate a ferric/ferrous ratio were excluded from the Fe^{2+} fit. For each cation, robust linear least-squares fits to the M^{2+}–Mg exchange using the data from Takahashi (1978) are shown as continuous lines (T78). Similar fits for the M^{2+}–Mg exchange using the Filter-B dataset (Filter-B) are shown as dashed lines. Black filled circles are from this work.

that the structural environment of Ni in silicate liquids is poorly constrained and is, in any case, likely to be a function of temperature and composition (e.g. Galoisy & Calas, 1993). Nevertheless, the basic point remains that the olivine–liquid partitioning behavior of Ni appears to be fundamentally different from those of other cations in magmatic olivines.

ORIGIN OF HIGH-NiO OLIVINES IN MAFIC IGNEOUS ROCKS

Calculation fundamentals

Previous workers have concluded that it is difficult to generate olivine phenocrysts with Ni concentrations significantly higher than those of olivine in the mantle source by low degrees of high-pressure partial melting followed by low-pressure crystallization (e.g. Sobolev *et al.*, 2005). This view is a direct consequence of assuming that $D_{Ni}^{ol/liq}$ is a function of only composition; that is, the Ni content of the first, most Ni-enriched, olivine to crystallize from a primary magma generated by peridotite melting must then be identical to that of the residual olivine in the source. If partial melting of an olivine-bearing source cannot account for the observed Ni enrichments in olivine phenocrysts for Hawaiian (and other) ocean-island basalts, then some other process must be involved, inspiring the variety of hypothesis described in the Introduction to explain their occurrence (e.g. Ryabchikov, 2003; Sobolev *et al.*, 2007). However, we showed above that $D_{Ni}^{ol/liq}$ is temperature dependent; in this section, we explore the consequences of this result for understanding the Ni contents of near-surface olivines crystallizing from primitive mantle-derived melts.

We model the process of partial melting in the mantle followed by crystallization of olivine phenocrysts as follows: at some depth, a partial melt separates from its residual mantle source; this melt then travels to the surface (or in the case of Hawaii, to a near-surface magma chamber) without changing composition; it then cools enough to begin crystallizing olivine phenocrysts. This simple approach requires two statements of olivine–liquid equilibrium, one for the source region and another for the near-surface conditions of phenocryst crystallization (but it does not require specifying the specific P–T cooling path taken by the melt in traveling from the source to the surface as long as the temperature stays above the melt's liquidus along the entire path). In this model, the NiO content of the primary partial melt is controlled by the NiO and forsterite contents of the olivine in the residual mantle, the MgO content of the melt, and the temperature of the source region [see equation (5)]. Likewise, the NiO content of the first olivine phenocryst to crystallize is controlled by the NiO and MgO contents of the primary melt, the forsterite content of the olivine phenocrysts [given the near constancy of the Fe^{2+}–Mg K_D over the relevant P–T range (see Fig. 4), the forsterite contents of the olivine phenocrysts and the residual olivines in the source are essentially identical], and the temperature at which near-surface crystallization begins. However, the positive P–T slopes of the liquidi of primitive basalts mean that the temperature of near-surface olivine phenocryst formation ($T_{surface}$) must be lower than the temperature at which the primary melt equilibrated with and separated from the residual mantle ($T_{separation}$). Equation (5) requires that $D_{Ni}^{ol/liq}$ be larger at the lower temperatures of olivine phenocryst growth, relative to $D_{Ni}^{ol/liq}$ during the high-temperature partial melting of the source. Consequently, we predict that early crystallizing olivines will be enriched in Ni relative to the olivines in their source, potentially explaining why forsteritic olivine phenocrysts are often enriched in Ni relative to olivines in mantle peridotites.

In the following subsections, we quantitatively connect the degree of Ni enrichment to the temperature difference, ΔT, between the magma source, $T_{separation}$, and the near-surface crystallization temperature, $T_{surface}$, of a phenocryst. We then use olivine–liquid equilibria to relate the ΔT required to explain a given degree of Ni enrichment to the pressure at which the primary melt separated from its source region. We also show for Hawaii that the observed NiO contents of magnesian olivines are consistent with Hawaiian primary magmas having separated from their source regions at the base of the lithosphere, assuming that the NiO concentrations of olivine in the source region are similar to those observed in spinel peridotites (Korenaga & Kelemen, 2000). Although other processes such as those that have been proposed previously to account for Ni-rich olivine phenocrysts may well occur, our treatment indicates that they are not required to account for Ni enrichment of magnesian olivines in ocean island basalts from Hawaii and elsewhere.

Ocean-island magmas

Magnesian olivine phenocrysts in Hawaiian tholeiites have some of the highest Ni contents measured in basaltic magmas (e.g. Clague *et al.*, 1991; Sobolev *et al.*, 2005, 2007). To illustrate how a temperature-dependent Ni partition coefficient affects the Ni contents of magnesian phenocrysts, we selected 18 estimates of parental (or primary) melt compositions from Mauna Loa, Mauna Kea and Kilauea (Wright, 1984; Clague *et al.*, 1991; Baker *et al.*, 1996; Herzberg & O'Hara, 2002; Stolper *et al.*, 2004; Herzberg, 2006; Matzen *et al.*, 2011) for which MgO ranges from 16 to 22 wt % (selected compositions are listed in the Supplementary Material). We assume these melts to have a water content of 0·4 wt % (after Clague *et al.* 1995), and that olivine phenocrysts form at a pressure of 0·2 GPa (~6 km; Roedder, 1983; Kauahikaua *et al.*, 2000). Liquidus temperatures calculated using equation (15) of Putirka (2008) range from 1361 to 1467°C (1420°C for the melt with the median MgO content). The compositions of olivine in equilibrium with these liquids were calculated assuming an oxygen fugacity two log units below the QFM buffer (rapidly quenched Mauna Loa lavas suggest an oxidization state of ~QFM − 1·8; Rhodes & Vollinger 2005), the ferric/ferrous expression of O'Neill *et al.* (2006), and a $K_{D,Fe^{2+}-Mg} = 0{\cdot}34$. Mg# values of the olivines range from 88·5 to 91·4, which compares favorably with the most Mg-rich olivines found in Hawaii (Mg# values of 90·8, 91·7 and 91·0 for Kilauea, Mauna Loa, and Mauna Kea, respectively; see Matzen *et al.*, 2011).

First, we consider a calculation in which a residual mantle olivine at melt segregation has 0·37 wt % NiO, the mean global value for olivines from spinel peridotites (Korenaga & Kelemen, 2000). We assume that this value is independent of $T_{separation}$ [i.e. 3 GPa partial melting calculations on mantle peridotite using BATCH (Longhi, 2002) predict that residual olivine Ni contents are relatively constant to more than 30% partial melting]. Figure 5 shows the calculated NiO contents for near-surface olivines as a function of ΔT (i.e. $T_{separation} - T_{surface}$). Each primary liquid produces a different relationship between ΔT and NiO in the phenocryst olivine but all are encompassed by the gray shaded region in Fig. 5; the black line represents the composition with the median MgO content (19·02 wt %): the liquidus for this composition is 1420°C at 0·2 GPa [equation (15) of Putirka (2008)] and the Mg# of the olivine is 90·1. If ΔT is zero (i.e. $T_{separation}$ and $T_{surface}$ are the same), $D_{Ni}^{ol/liq}$ at $T_{surface}$ and $D_{Ni}^{ol/liq}$ at $T_{separation}$ are equal, and, because the melt composition is unmodified prior to crystallization of the near-surface phenocryst, the near-surface olivine recovers the mantle olivine value (i.e. 0·37 wt % NiO). As ΔT increases, the computed value of $T_{separation}$ must increase because $T_{surface}$ is fixed. This leads to a decrease in $D_{Ni}^{ol/liq}$ at $T_{separation}$, which results in a higher Ni content of the melt and a corresponding increase in the NiO content of the near-surface olivine.

There are two insets in Fig. 5. In the upper left is a histogram of the NiO contents for high-Mg (Mg# ≥89)

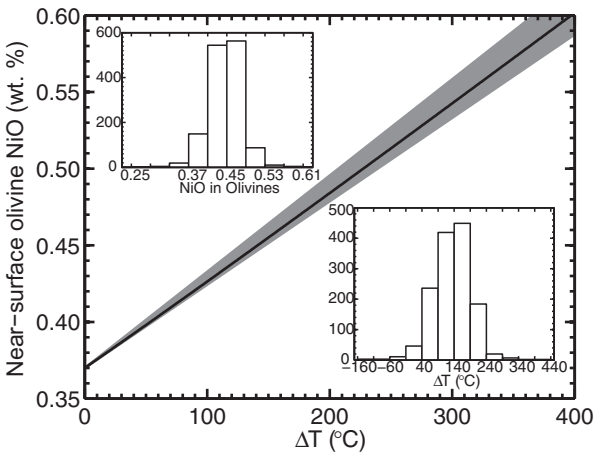

Fig. 5. Calculated NiO in near-surface olivine vs ΔT for Hawaiian magmas. For each estimated primary or parental melt, we calculate the NiO content of the low-pressure (0·2 GPa) olivine as a function of the temperature difference (ΔT) between the crystallization temperature at low pressure [estimated using Putirka (2008), equation (15)] and the separation of the melt from the residual mantle. We assume that the residual mantle olivine has a constant composition of 0·37 wt % NiO and use the coefficients for equation (5) derived from a fit of the Filter-B dataset. The gray triangular-shaped region in the figure encompasses results for all of the estimated primary liquid compositions, and the black line represents the composition whose MgO content is nearest to 19·02 wt % MgO (Matzen *et al.*, 2011). Insets are a histogram of NiO contents of high-Mg (Mg# values ≥89) olivines from Mauna Loa, Mauna Kea and Kilauea volcanoes reported by Sobolev *et al.* (2007) and the corresponding calculated ΔT for those olivines, using the near-median parental liquid composition. A ΔT of ~150°C corresponds to a melt that separated from the residual mantle at ~2·7 GPa, close to the estimated pressure of the base of the lithosphere beneath Hawaii, ~2·9 GPa).

olivines from Mauna Kea, Mauna Loa and Kilauea reported by Sobolev *et al.* (2007). The olivines show a well-defined central peak at 0·45 wt % NiO, with most grains exhibiting concentrations in the range 0·39–0·50 wt %. Keeping NiO in the source olivine at 0·37 wt % and choosing the median estimated parental liquid (black line in Fig. 5), we can calculate ΔT for each of these olivine phenocryst compositions and this leads to the inset histogram in the lower right of Fig. 5. The median value for ΔT is 136°C, with a range from −147 to 400°C.

Setting aside for the moment the physical reality of the extreme ΔT values shown in Fig. 5, we first consider the physical significance of the median ΔT, 136°C. We can connect ΔT to a depth of origin by noting that (1) olivine is saturated in both the source region and at the site of low-pressure crystallization of the phenocrysts, and (2) the melt composition is the same for both locations. Sugawara (2000) estimated the slope of the liquidus for an olivine-saturated melt of constant MgO to be 55°C GPa^{-1}, essentially equivalent to the value predicted by MELTS for the primary melt composition MK1 from Matzen *et al.* (2011), which gives ∼56°C GPa^{-1}, between 1·0 and 2·0 GPa, and by equation (4) of Putirka *et al.* (2007), which yields ∼54°C GPa^{-1}. We take 55°C GPa^{-1} as a reasonable slope, so 136°C leads to a predicted pressure difference between the source from which the primary liquid was extracted and the shallow-level chamber where the initial phenocryst grew of 2·5 GPa. Because the shallow-level chamber is at ∼0·2 GPa, as noted above, our simple calculation predicts a pressure at the source of 2·7 GPa, very close to the estimated pressure at the base of the lithosphere beneath Hawaii (2·9 GPa; Priestley & Tilmann, 1999). Taken at face value, our simple calculation suggests that primary Hawaiian magmas separate from their source region at or near the base of the lithosphere. If the thickness of the lithosphere controls the pressure, and therefore the temperature of melt segregation ($T_{separation}$), a thinner lithosphere implies a smaller ΔT and, provided NiO content in the source olivines are the same, a lower NiO concentration in the most magnesian olivine phenocrysts. Thus, Iceland, which is built on a lithosphere that is thin compared with that under Hawaii, would be expected—and is observed (e.g. fig. 1 of Sobolev *et al.*, 2005)—to have lower NiO contents in magnesian olivine phenocrysts. As noted by Sobolev *et al.* (2007), olivine phenocrysts in lavas erupted onto 'thick' lithosphere tend to have higher NiO contents than those erupted onto 'thin' lithosphere; this is consistent with qualitative expectations based on Fig. 5.

In the calculations presented above for Hawaii, we focused on the difference in temperature (and pressure) between the source and shallow-level reservoir within which the parental liquid begins to crystallize. We did this because Ni contents in olivine are more sensitive to ΔT than they are to absolute T (but see next section). However, the selection of specific parental liquid implies a specific, model-dependent $T_{surface}$, and therefore ΔT carries a constraint on $T_{separation}$. For example, the illustrative parental melt described above yields $T_{surface} = 1420$°C, according to equation (15) of Putirka (2008), so that ΔT of 136° leads to $T_{separation} = 1556$°C. Calculations using MELTS lead to a higher source temperature, $T_{separation} = 1605$°C, and calculations using the MgO-based thermometer of Helz & Thornber (1987), which is optimized for Kilauea, yield a lower value, $T_{separation} = 1532$°C. The 1530 and 1540°C experiments of Walter (1998) at 3 GPa on a fertile peridotite produced liquids with 17·6 and 18·2 wt % MgO at melt fractions of 18·5 and 24·4 wt %, respectively. These results are in reasonable agreement with source temperatures calculated using Helz & Thornber (1987) and equation (15) of Putirka (2008), and are therefore consistent with batch melting of fertile peridotite beneath Hawaii. The source temperature obtained via MELTS is too high relative to expectations based on the experiments of Walter (1998). One possible explanation is that MELTS correctly predicts the temperature for the onset of olivine crystallization for our representative primary melt but the selected primary melt is too magnesian. There are, however, many variables that enter into the calculation of a primary liquid. For example, $T_{surface}$ is lower for lower MgO (by ∼20° per wt % MgO) but it is also lower for higher H_2O [by 13° per wt % H_2O, according to equation (15) of Putirka (2008), although this may well underestimate the effect (Médard *et al.*, 2008)] and more reducing conditions (by ∼20° per log unit in fO_2). Decreasing the Mg# of the source olivine also lowers $T_{surface}$. There is also a significant trade-off between ΔT and the NiO content of the source olivine, as discussed below (see also Fig. 5). Thus, many parameters need to be considered in optimizing constraints on source conditions and parental melt chemistry and it is beyond the scope of this study to choose a single 'best' guess from among the proposed parental magmas listed in Supplementary Material Table S2 or to create a new one. However, the key point is unaffected by those choices: forsteritic olivine phenocrysts are expected to be Ni-rich relative to the residual olivines in the mantle sources of their parental magmas, based on the temperature dependence of Ni partitioning reported here, and the expected magnitude of Ni enrichment is very similar to what is observed for Hawaiian olivines.

In the above discussion, we made the simplifying assumption that olivine in the mantle source has a constant concentration of 0·37 wt %, the average for spinel peridotites observed by Korenaga & Kelemen (2000). When applied to observed Hawaiian phenocrysts, this leads to a median predicted ΔT of 136°C, which is consistent with the derivation of primary liquids near the base of the lithosphere. However, it also leads to values of ΔT as high as

400°C for the most Ni-rich olivines, implying that melt separated from the residual mantle at great depths, and $\Delta T < 0$, implying that (if no fractionation has taken place) the primary liquids entering shallow reservoirs beneath Hawaii are hotter than they were in the source region. These extreme results may be a consequence of assuming a constant concentration of NiO in olivine in the mantle source. This assumption is unlikely to be correct in detail: the bulk NiO content of the source region of other mantle plumes is inferred to vary (e.g. Shorttle & Maclennan, 2011), as do the NiO contents of olivine in spinel peridotites, 0·18–0·56 wt %, from the data of Korenaga & Kelemen (2000). To illustrate the importance of source olivine composition, we consider a primitive melt extracted at 2·9 GPa (i.e. the base of the lithosphere) that rises without chemical modification to 0·2 GPa, where an olivine phenocryst crystallizes; estimating the slope of the olivine-saturated liquidus to be 55°C GPa^{-1}, this corresponds to a ΔT of 149°C. Other variables are defined as above, except that we now assume mantle olivines to have a distribution of NiO contents equal to that of the high-Mg olivines (Mg# $\geq$ 89) from the compilation by Korenaga & Kelemen (2000) of spinel peridotites. In essence, we are predicting what the distribution of NiO contents of magnesian, near-surface (0·2 GPa) olivine phenocrysts should look like, assuming that partial melting takes place at the base of the lithosphere and that spinel peridotites from the database of Korenaga & Kelemen (2000) are representative of the distribution in the source region under Hawaii. Calculated NiO contents in magnesian olivine phenocrysts are shown in the form of a histogram (filled gray bars) in Fig. 6 normalized to a sum of unity. This distribution is overlain on the normalized distribution of observed magnesian olivine phenocrysts (open bars) from Sobolev *et al.* (2007). The median (0·46 wt % NiO predicted vs 0·45 observed), mean (0·46 vs 0·45), and the mean absolute deviation, MAD (0·031 vs 0·026) are virtually identical. The range is larger for the predicted values (0·22–0·68 vs 0·28–0·60) and the distribution of the natural olivines is slightly skewed to low NiO values relative to the calculated distribution. These differences may be due to the fractionation of olivine from primitive melts, sampling biases in one or both of the spinel peridotite and olivine phenocryst populations, or failures in one or more of the assumptions used for the calculation. For example, the length scales of the variation in NiO contents of olivine in the mantle under Hawaii need to be large enough for them to be expressed by partial melting (e.g. Kogiso *et al.*, 2004). Additionally, the pressure and temperature of the residual source may be poorly defined if parental melts are mixtures derived from various depths (e.g. Sobolev *et al.*, 2000; Norman *et al.*, 2002), and there is also likely to be some variation in source composition (e.g. Mg#). It is also possible that parental liquids

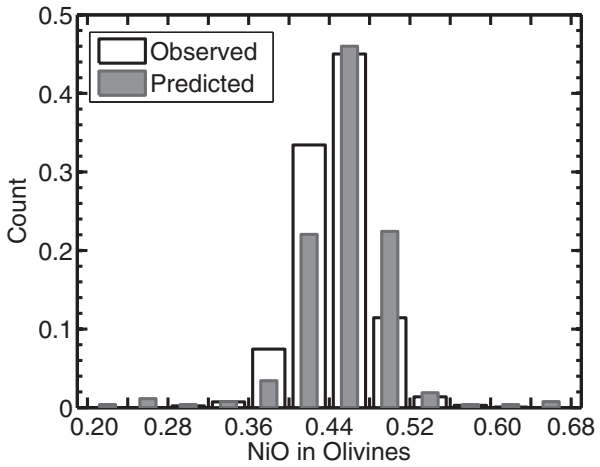

Fig. 6. Histogram of olivine NiO concentrations in the source region under Hawaii. Thin gray bars represent the distribution (sum normalized to unity) of predicted olivine compositions assuming that ΔT is 149°C (equivalent to the melt separating from the residual mantle at the base of the lithosphere) and that the distribution of NiO content of the olivine in the mantle residue is equal to that of the high-Mg (Mg# values ≥89) olivines from spinel lherzolites reported by Korenaga & Kelemen (2000). Calculations are for the median (based on MgO) primary liquid from Matzen *et al.* (2011), which yielded the continuous black line in Fig. 5. Also shown, with wider white bars, is the normalized distribution of olivine NiO contents for high-Mg olivines from Mauna Loa, Mauna Kea, and Kilauea volcanoes reported by Sobolev *et al.* (2007). Predicted olivine NiO contents encompass the entire range of observed olivines and display a similar distribution. The implied NiO content of primary melts for these calculations is tightly bounded with a median of 0·097 wt % NiO and an MAD of 0·007.

reequilibrate as they travel to the surface; that is, were the melt to equilibrate with mantle olivine as it ascended from its source, it would change in composition continuously, always in equilibrium with olivine that had, for example, 0·37 wt % NiO. The presence of both low- and high-silica magmas erupted from Mauna Kea (Rhodes & Vollinger, 2004; Stolper *et al.*, 2004) as well as the diversity of melt inclusion compositions in Hawaiian olivines (e.g. Sobolev *et al.*, 2000), suggests that mantle melts can traverse the lithosphere without losing their distinctive geochemical characteristics, but some changes may well occur.

These two calculations also serve to illustrate that to produce an olivine with a given NiO content, there is a tradeoff between ΔT and the NiO content of the olivine in the source. For a calculated ΔT to have significance we must know, or at least be able to approximate, the NiO contents of the olivines in the source. With that in mind, we cannot rule out alternative hypotheses for producing the high-Ni olivines observed in Hawaii and elsewhere (e.g. Ryabchikov, 2003; Sobolev *et al.*, 2007) or the superimposition of these alternative hypotheses and the effects of a temperature-dependent $D_{Ni}^{ol/liq}$. However, if the Ni contents of olivines from peridotites are representative of those in the mantle, our results suggest a basic

self-consistency between the depth of origin for primary Hawaiian melts and Ni contents of magnesian phenocrysts in Hawaiian lavas.

Komatiites

In the previous subsection, we demonstrated that high Ni contents in magnesian olivines from Hawaii are consistent with their crystallization at shallow levels (0·2 GPa) from primary melts that were extracted from the base of the lithosphere at ~2·9 GPa. Komatiites are also thought to represent partial melts of the mantle, but the depths of origin and the nature of the source regions are much less well constrained. Observed NiO contents of komatiitic olivines of a given Mg# are generally lower than those in Hawaiian lavas (e.g. Sobolev *et al.*, 2005), as is the maximum, ~0·51 wt % for komatiites (Arndt *et al.*, 2008, and references therein) versus 0·60 wt % NiO for magnesian Hawaiian olivine phenocrysts (e.g. Sobolev *et al.*, 2005). Komatiites are generally thought to have erupted at high temperatures (~1600°C; Huppert & Sparks, 1985; Nisbet *et al.*, 1993; Herzberg *et al.*, 2007; Arndt *et al.*, 2008) relative to the temperatures at which forsteritic olivines crystallize at low pressure from primitive Hawaiian basalts (1420°C for the composition considered in the previous section). In this subsection, we first consider the importance of temperature for Ni enrichment in early crystallizing olivine in komatiites vis à vis expectations based on Hawaiian primary magmas. We show that, when compared with Hawaiian magmas, the higher eruption temperature for komatiites leads to less extreme Ni enrichments in low-pressure olivine phenocrysts relative to source-olivine compositions. As a result, Ni contents of forsteritic olivines in komatiites are consistent with reasonable estimates of the temperature difference between their source and the crystallization of phenocrysts at the Earth's surface. We also show that inferred values of ΔT can, in principle, be used to constrain the pressure of the source region.

We begin, as before, with equation (5) and first isolate the effect of temperature. This is an important consideration because komatiites (excluding the picritic komatiites of Gorgona) are generally thought to have been much hotter than basalts when olivine began to crystallize, ~1600°C or higher (Nisbet *et al.*, 1993; Herzberg *et al.*, 2007; Arndt *et al.*, 2008), versus roughly 1375–1500°C for primitive Hawaiian magmas (see previous section, and Matzen *et al.*, 2011). Taking two olivines of the same Mg# that are in equilibrium with melts of identical composition but differing in temperature (i.e. at different pressures along the liquidus of a given liquid, we subtract the pair of equation (5)s describing the partitioning of Ni to obtain

$$\frac{X^{\mathrm{molar}}_{\mathrm{NiSi_{0.5}O_2}}(T_1)}{X^{\mathrm{molar}}_{\mathrm{NiSi_{0.5}O_2}}(T_2)} = \exp\left[\frac{\Delta_{r(1)}H^{\circ}_{T_{\mathrm{ref}},P_{\mathrm{ref}}}}{R}\left(\frac{1}{T_2}-\frac{1}{T_1}\right)\right]. \quad (8)$$

Equation (8) indicates that the olivines will differ in Ni concentrations to the extent that $\Delta_{r(1)}H^{\circ}_{T_{\mathrm{ref}},P_{\mathrm{ref}}}$ is nonzero and that this difference scales with the difference in inverse temperature. For the same temperature difference (i.e. $T_1 - T_2$ is constant), the difference in inverse temperature $(1/T_1) - (1/T_2)$ is smaller for a hotter magma. Thus, because $\Delta_{r(1)}H^{\circ}_{T_{\mathrm{ref}},P_{\mathrm{ref}}}$ is negative (Table 4), the degree of Ni enrichment in olivines crystallizing from komatiitic melts near the Earth's surface will be smaller than in those in cooler primary Hawaiian basaltic liquids. The effect is modest but significant. The primary Hawaiian melt described above has a liquidus temperature of 1420°C at 0·2 GPa. According to equation (8), a near-surface magnesian olivine crystallizing from this liquid will be enriched in NiO by a factor of 1·23 relative to olivine in the source if ΔT is 150°C. For the same 150°C ΔT, a komatiite in which the initial olivine crystallized at 1600°C would show a NiO enrichment factor of only 1·19. Thus, other things being equal, Ni contents of initially crystallizing komatiite olivines will be lower than those in ocean island basalts, by ~0·02 wt % NiO [taking 0·37 wt % NiO for source olivine, the average value for the spinel peridotites of Korenaga & Kelemen (2000), as the basis for computing wt % values]. The median NiO for magnesian olivines in komatiites is 0·43 wt % NiO and the corresponding value in Hawaiian samples is 0·45 (Sobolev *et al.*, 2007); that is, a difference of 0·02 wt % NiO, the same as our calculated value. In detail, other factors are probably important, especially if the hydrous melting model of Grove and coworkers (e.g. Grove & Parman, 2004; Parman *et al.*, 2004; Barr *et al.*, 2009) is correct. Nevertheless, this simple calculation demonstrates that high absolute temperatures for komatiites should translate into lower Ni enrichments in the early crystallizing olivine relative to ocean island basalts, with predicted differences similar to those observed in nature.

For the Hawaiian example discussed in the preceding section, we were able to connect the depth of the source region with the observed Ni contents of magnesian olivine phenocrysts and olivines in spinel peridotites. For komatiites, we know considerably less about the nature of their source regions or their depths. Estimates for the pressure of the source region range from ~2·5 to >10 GPa for Archaean komatiites, and the composition of the source region, including volatile contents, of komatiitic magmas remains contentious (e.g. Grove & Parman, 2004; Arndt *et al.*, 2008). We therefore approach komatiites primarily from the surface and attempt to constrain conditions in the source region using procedures similar to those described for Hawaii in the previous section. The principal difference in our treatment of komatiites is that we treat NiO in the parental melt as a known and calculate NiO in source olivine as a function of ΔT. For a parental liquid composition, we use Barberton komatiite K4-1BA, which

was analyzed by Parman *et al.* (2004) and interpreted to be a liquid by Arndt *et al.* (2008). Assuming an fO_2 of QFM − 2 and an emplacement pressure of 1 atm, MELTS calculations suggest that olivine with a Mg# of 94 is on the liquidus at 1610°C. These MELTS predictions agree well with the Mg# of the most Mg-rich phenocryst observed in the formation, also 94 (Parman *et al.*, 2004), and with the estimated eruption temperature of 1600°C (Arndt *et al.*, 2008). From Parman *et al.* (2004), the bulk NiO concentration of K4-1BA is 0·213 wt % (after converting Fe_2O_3 in the analysis to FeO* and renormalizing), twice the concentration inferred above for a Hawaiian primary melt. This presumably reflects a lower $D_{Ni}^{ol/liq}$ during partial melting of the source and perhaps a higher degree of partial melting (e.g. Viljoen & Viljoen, 1969; Bickle *et al.*, 1977). Provided the Mg# of the source olivine is the same as that of the 1 atm liquidus olivine and that the primary melt was not modified during ascent [komatiites are thought to have erupted rapidly (e.g. Peslier *et al.*, 2008)], we can compute the NiO content of olivine in the source as a function of ΔT.

Figure 7a shows the relationship between NiO contents of olivine in the source region and ΔT for Barberton komatiite K4-1BA. If we assume that there is 0·37 wt % NiO in olivine in the source, the average for spinel peridotites of Korenaga & Kelemen (2000) [high-MgO olivines from garnet peridotites reported by Korenaga & Kelemen (2000) have a median of 0·38], then a ΔT of 331°C is predicted with a range between 262 and 399°C, assuming that a 6% (2σ) error (e.g. Gazulla *et al.*, 2010) is appropriate for the Parman *et al.* (2004) XRF analysis of K4-1BA. These temperatures are considerably higher than the 136°C we calculated above for a Hawaiian primary liquid. At face value, this suggests a hotter mantle or a deeper source, but we also note that there is a direct trade-off between ΔT and the inferred NiO contents of olivine in the source, so if the olivine in the mantle source from which komatiites were generated was more Ni-rich than indicated by spinel peridotites, lower ΔT values would be implied. Also, if the NiO content of K4-1BA given by Parman *et al.* (2004) is not representative of the parental melt, different ΔT values would be obtained.

If we accept 0·37 wt % NiO in olivine as representative of the komatiite source region and have a relationship between ΔT and pressure for a primary liquid, then we can estimate pressure in the source region using the same approach that we developed above for Hawaii. The phase relations of K4-1BA, our putative primary melt, have not been determined experimentally, so we computed the liquidus as a function of pressure for this bulk composition using MELTS, with the results shown in Fig. 7b. These calculated olivine-saturated liquidus temperatures are similar to the trace of the olivine liquidus for a less magnesian komatiite, AUK, studied experimentally by Wei *et al.* (1990),

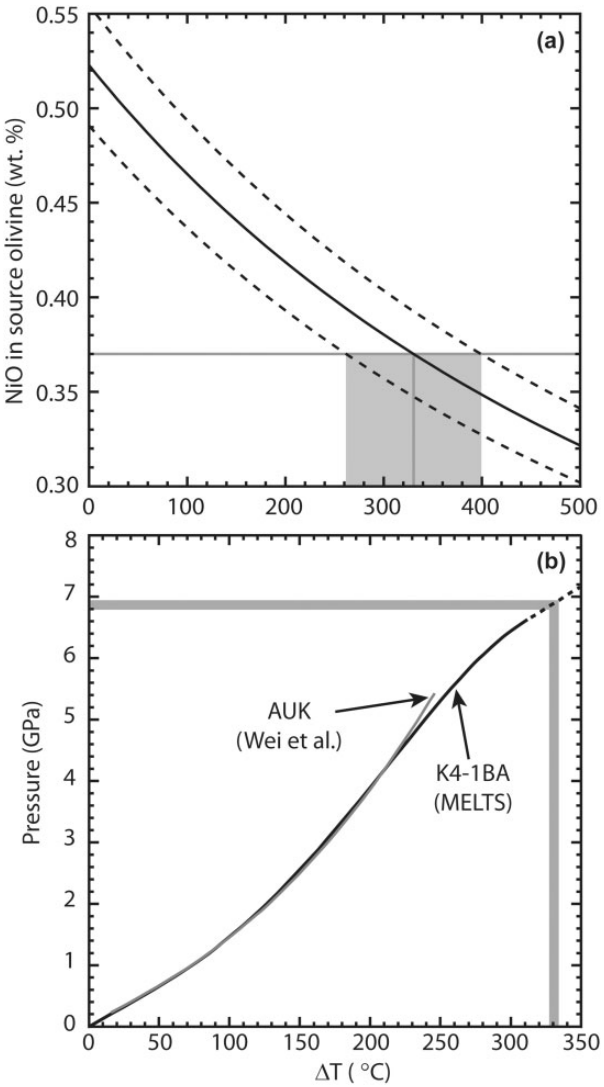

Fig. 7. (a) NiO of source olivine (continuous curve) as a function of ΔT for Barberton komatiite K4-1BA, reported by Parman *et al.* (2004) and interpreted to be a liquid by Arndt *et al.* (2008) with dashed curves indicating ±6% errors for the XRF determination of bulk NiO. For a mantle olivine with 0·37 wt % NiO, $\Delta T = 331 \pm 69$°C. (b) Pressure (GPa) as a function of ΔT for K4-1BA based on MELTS calculations of olivine–liquid equilibria, suppressing other phases. The curve is extrapolated above 6·5 GPa. If $\Delta T = 331$°C, a pressure of ~7 GPa is implied. Also shown as a gray curve is a combination of MELTS calculations (<4·0 GPa) and the trace of the olivine–liquidus curve from the phase diagram for AUK (≥4·0 GPa), an Al undepleted komatiite bulk composition studied by Wei *et al.* (1990).

which is also shown. Based on $\Delta T = 331$°C for K4-1BA and the calculated olivine liquidus temperatures according to MELTS, the source pressure was roughly 7 GPa, although there are large uncertainties (see Fig. 7a; $\Delta T = 262$°C leads to 5·6 GPa and 399°C to 7·9 GPa). For a second bulk composition, ADK, studied by Wei *et al.* (1990), the MELTS calculated liquidus and the experimentally determined

values are offset by ~25°C. This makes it difficult to quantify ΔT but, because $\Delta T/\Delta P$ decreases faster at high pressures for the ADK experiments than suggested by MELTS calculations for the AUK composition, it would lead to higher estimates of the pressure in the source region. Our results suggest a deep origin (~7 GPa), lower in pressure than recent estimates for the conditions at which komatiitic melts separate from the residual mantle (9–13 GPa, Robin-Popieul *et al.*, 2012). There are, however, a number of reasons why our komatiite calculations should be regarded as only semi-quantitative. The phase relations for komatiitic liquids are poorly constrained at high pressures, and to produce the MELTS curve shown in Fig. 7b it was necessary to suppress crystallization of orthopyroxene, clinopyroxene and garnet. For pressures as high as 7 GPa, our assumption that equation (5) is independent of pressure may well break down, and the solid–solid and solid–liquid Ni partition coefficients at such extreme pressures (and temperatures) are not well known. Finally, we note that the pressure calculation assumes a dry magma and takes no account of the possible influence of volatiles on the phase relations for komatiites and, in particular, of the relationship between the temperature of the olivine liquidus and pressure.

CONCLUSIONS

We conducted olivine–liquid partitioning experiments on roughly constant liquid compositions over a range of pressures (1 atm–3 GPa) and temperatures (1400–1550°C) to determine the effect of temperature on Ni partitioning between olivine and melt. Models that ascribe variations in $D_{Ni}^{ol/liq}$ solely to differences in liquid composition or solely to temperature are inconsistent with the results of our experiments. Our work, which held the liquid composition approximately constant, has shown that changes in temperature can have a significant effect on the observed partition coefficients. Our data, as well as those from the literature, are fitted well by a simple thermodynamic expression where $D_{Ni}^{ol/liq}$ is a function of temperature, olivine and liquid composition.

Based on a simple model in which partial melting to produce a primary liquid and subsequent crystallization of that liquid take place at two different pressures and temperatures, the increase in $D_{Ni}^{ol/liq}$ with decreasing temperature predicts the crystallization of low-pressure olivine phenocrysts with higher NiO contents than the olivines in the source region. Observed NiO concentrations of magnesian olivine phenocrysts from Mauna Loa, Mauna Kea and Kilauea are consistent with derivation from primary partial melts produced at the base of the lithosphere ($\Delta T = 149$°C; 2·9 GPa) from peridotites in which olivines have a distribution of NiO concentrations equal to that observed in spinel peridotites. The lower levels of NiO enrichment observed in komatiitic olivines relative to magnesian olivine phenocrysts from Hawaii could reflect the higher temperatures associated with komatiites; for one suggested primary Baberton komatiite liquid, simple calculations based on observed NiO enrichments suggest a deep (~7 GPa) origin.

ACKNOWLEDGEMENTS

We thank Glenn Gaetani and Russ Colson for providing insights into their work, Ma Chi for guidance on the electron microprobe, Paul Asimow and Paula Antoshechkin for help with the MELTS calculations, Jun Korenaga for supplying data, and F. Davis, J. Maclennan, and K. Putirka for thoughtful reviews.

FUNDING

Funding was provided by National Science Foundation grant EAR-1019886, National Aeronautics and Space Administration grant NNG04GG14G, and European Research Council grant 267764.

SUPPLEMENTARY DATA

Supplementary data for this paper are available at *Journal of Petrology* online.

REFERENCES

Agee, C. B. & Walker, D. (1990). Aluminum partitioning between olivine and ultrabasic silicate liquid to 6 GPa. *Contributions to Mineralogy and Petrology* **105**, 243–254.

Ai, Y. & Lange, R. A. (2008). New acoustic velocity measurements on $CaO–MgO–Al_2O_3–SiO_2$ liquids: Reevaluation of the volume and compressibility of $CaMgSi_2O_6–CaAl_2Si_2O_8$ liquids to 25 GPa. *Journal of Geophysical Research* **113**, B04203, doi:10.1029/2007JB005010.

Albarède, F. & Provost, A. (1977). Petrological and geochemical mass-balance equations: an algorithm for least-square fitting and general error analysis. *Computers and Geosciences* **3**, 309–26.

Armstrong, J. T. (1988). Quantitative analysis of silicate and oxide minerals: comparison of Monte Carlo, ZAF and $\phi(\rho z)$ procedures. In: Newbury, D. E. (ed.) *Microbeam Analysis—1988*. San Francisco Press, pp. 239–246.

Arndt, N. T. (1977). Partitioning of nickel between olivine and ultrabasic and basic komatiite liquids. *Carnegie Institution of Washington Year Book* **76**, 553–557.

Arndt, N. (2008). *Komatiite*. Cambridge University Press.

Baker, M. B., Alves, S. & Stolper, E. M. (1996). Petrography and petrology of the Hawaii Scientific Drilling Project lavas: Inferences from olivine phenocryst abundances and compositions. *Journal of Geophysical Research* **101**, 11715–11727.

Baker, M. B., Matzen, A. K., Lesher, C. E. & Stolper, E. M. (2009). The influence of phase equilibria on mineral Fe/Mn ratios in mantle peridotite. *EOS Transactions American Geophysical Union, Fall Meeting Supplement* **90**, Abstract V31D-1998.

Barr, J. A., Grove, T. L. & Wilson, A. H. (2009). Hydrous komatiites from Commondale, South Africa: An experimental study. *Earth and Planetary Science Letters* **284**, 199–207.

Bass, J. D., Weidner, D. J., Hamaya, N., Ozima, M. & Akimoto, S. (1984). Elasticity of the olivine and spinel polymorphs of Ni_2SiO_4. *Physics and Chemistry of Minerals* **10**, 261–272.

Beattie, P. (1993*a*). Olivine–melt and orthopyroxene–melt equilibria. *Contributions to Mineralogy and Petrology* **115**, 103–111.

Beattie, P. (1993*b*). On the occurrence of apparent non-Henry's Law behaviour in experimental partitioning studies. *Geochimica et Cosmochimica Acta* **57**, 47–55.

Beattie, P., Ford, C. & Russell, D. (1991). Partition coefficients for olivine–melt and orthopyroxene–melt systems. *Contributions to Mineralogy and Petrology* **109**, 212–224.

Berman, R. G. (1988). Internally-consistent thermodynamic data for minerals in the system Na_2O–K_2O–CaO–MgO–FeO–Fe_2O_3–Al_2O_3–SiO_2–TiO_2–H_2O–CO_2. *Journal of Petrology* **29**, 445–522.

Berman, R. G. & Aranovich, L. Y. (1996). Optimized standard state and solution properties of minerals I. Model calibration for olivine, orthopyroxene, cordierite, garnet, ilmenite in the system FeO–MgO–CaO–Al_2O_3–TiO_2–SiO_2. *Contributions to Mineralogy and Petrology* **126**, 1–24.

Bickle, M. J., Ford, C. E. & Nisbet, E. G. (1977). The petrogenesis of peridotitic komatiites: Evidence from high-pressure melting experiments. *Earth and Planetary Science Letters* **37**, 97–106.

Burns, R. G. & Fyfe, W. S. (1966). Behaviour of nickel during magmatic crystallization. *Nature* **210**, 1147–1148.

Campbell, I. H., Naldrett, A. J. & Roeder, P. L. (1979). Nickel activity in silicate liquids: some preliminary results. *Canadian Mineralogist* **17**, 495–505.

Chase, M. W. (ed.) (1998). *NIST–JANAF Thermochemical Tables*, 4th edn. American Institute of Physics.

Chen, G. Q., Ahrens, T. J. & Stolper, E. M. (2002). Shock-wave equation of state of molten and solid fayalite. *Physics of the Earth and Planetary Interiors* **134**, 35–52.

Clague, D. A., Weber, W. S. & Dixon, J. E. (1991). Picritic glasses from Hawaii. *Nature* **353**, 553–556.

Clague, D. A., Moore, J. G., Dixon, J. E. & Friesen, W. B. (1995). Petrology of submarine lavas from Kilauea's Puna Ridge, Hawaii. *Journal of Petrology* **36**, 299–349.

Colson, R. O., McKay, G. A. & Taylor, L. A. (1988). Temperature and composition dependencies of trace element partitioning: Olivine/melt and low-Ca pyroxene/melt. *Geochimica et Cosmochimica Acta* **52**, 539–553.

Davidson, P. M., Grover, J. & Lindsley, D. H. (1982). $(Ca,Mg)_2Si_2O_6$ clinopyroxenes: A solution model based on nonconvergent site-disorder. *Contributions to Mineralogy and Petrology* **80**, 88–102.

Dixon, J. E., Stolper, E. M. & Holloway, J. R. (1995). An experimental study of water and carbon dioxide solubilities in mid-ocean ridge basaltic liquids. Part I: Calibration and solubility models. *Journal of Petrology* **36**, 1607–1631.

Drake, M. J. & Holloway, J. R. (1981). Partitioning of Ni between olivine and silicate melt: The 'Henry's Law problem' reexamined. *Geochimica et Cosmochimica Acta* **45**, 431–437.

Duke, J. M. (1976). Distribution of the period four transition elements among olivine, calcic clinopyroxene and mafic silicate liquid: experimental results. *Journal of Petrology* **17**, 499–521.

Elthon, D. & Scarfe, C. M. (1984). High-pressure phase equilibria of a high-magnesia basalt and the genesis of primary oceanic basalts. *American Mineralogist* **69**, 1–15.

Falloon, T. J., Danyushevsky, L. V., Ariskin, A., Green, D. H. & Ford, C. E. (2007). The application of olivine geothermometry to infer crystallization temperatures of parental liquids: Implications for the temperature of MORB magmas. *Chemical Geology* **241**, 207–233.

Filiberto, J., Jackson, C., Le, L. & Treiman, A. H. (2009). Partitioning of Ni between olivine and an iron-rich basalt: Experiments, partition models, and planetary implications. *American Mineralogist* **94**, 256–261.

Fine, G. & Stolper, E. (1986). Dissolved carbon dioxide in basaltic glasses: concentrations and speciation. *Earth and Planetary Science Letters* **76**, 263–278.

Ford, C. E., Russell, D. G., Craven, J. A. & Fisk, M. R. (1983). Olivine–liquid equilibria: Temperature, pressure and composition dependence of crystal/liquid cation partition coefficients for Mg, Fe^{2+}, Ca and Mn. *Journal of Petrology* **24**, 256–265.

Gaetani, G. A. & Grove, T. L. (1997). Partitioning of moderately siderophile elements among olivine, silicate melt, and sulfide melt: Constraints on core formation in the Earth and Mars. *Geochimica et Cosmochimica Acta* **61**, 1829–1846.

Galoisy, L. & Calas, G. (1993). Structural environment of nickel in silicate glass/melt systems: Part 1. Spectroscopic determination of coordination states. *Geochimica et Cosmochimica Acta* **57**, 3613–3626.

Gazulla, M. F., Rodrigo, M., Vicente, S. & Orduña, M. (2010). Methodology for the determination of minor and trace elements in petroleum cokes by wavelength-dispersive X-ray fluorescence (WD-XRF). *X-Ray Spectrometry* **39**, 321–327.

Ghiorso, M. S. (2004). An equation of state for silicate melts. III. Analysis of stoichiometric liquids at elevated pressure: Shock compression data, molecular dynamics simulations and mineral fusion curves. *American Journal of Science* **304**, 752–810.

Ghiorso, M. S. & Sack, R. O. (1995). Chemical mass transfer in magmatic processes IV. A revised and internally consistent thermodynamic model for the interpolation and extrapolation of liquid–solid equilibria in magmatic systems at elevated temperatures and pressures. *Contributions to Mineralogy and Petrology* **119**, 197–212.

Ghiorso, M. S., Hirschmann, M. M., Reiners, P. W. & Kress, V. C. (2002). The pMELTS: A revision of MELTS for improved calculation of phase relations and major element partitioning related to partial melting of the mantle to 3 GPa. *Geochemistry, Geophysics, Geosystems* **3**, doi:10.1029/2001GC000217.

Grove, T. L. & Parman, S. W. (2004). Thermal evolution of the Earth as recorded by komatiites. *Earth and Planetary Science Letters* **219**, 173–187.

Häkli, T. A. & Wright, T. L. (1967). Fractionation of nickel between olivine and augite as a geothermometer. *Geochimica et Cosmochimica Acta* **31**, 877–884.

Hart, S. R. & Davis, K. E. (1978). Nickel partitioning between olivine and silicate melt. *Earth and Planetary Science Letters* **40**, 203–219.

Helz, R. T. & Thornber, C. R. (1987). Geothermometry of Kilauea Iki lava lake, Hawaii. *Bulletin of Volcanology* **49**, 651–668.

Henderson, C. M. B., Redfern, S. A. T., Smith, R. I., Knight, K. S. & Charnock, J. M. (2001). Composition and temperature dependence of cation ordering in Ni–Mg olivine solid solutions: a time-of-flight neutron powder diffraction and EXAFS study. *American Mineralogist* **86**, 1170–1187.

Herd, C. D. K., Dwarzski, R. E. & Shearer, C. K. (2009). The behavior of Co and Ni in olivine in planetary basalts: An experimental investigation. *American Mineralogist* **94**, 244–255.

Herzberg, C. (2006). Petrology and thermal structure of the Hawaiian plume from Mauna Kea volcano. *Nature* **444**, 605–609.

Herzberg, C. & O'Hara, M. J. (2002). Plume-associated ultramafic magmas of Phanerozoic age. *Journal of Petrology* **43**, 1857–1883.

Herzberg, C., Asimow, P. D., Arndt, N., Niu, Y., Lesher, C. M., Fitton, J. G., Cheadle, M. J. & Saunders, A. D. (2007). Temperatures in ambient mantle and plumes: Constraints from basalts, picrites, and komatiites. *Geochemistry, Geophysics, Geosystems* **8**, Q02006, doi:10.1029/2006GC001390.

Hesse, M. & Grove, T. L. (2003). Absarokites from the western Mexican Volcanic Belt: constraints on mantle wedge conditions. *Contributions to Mineralogy and Petrology* **146**, 10–27.

Hirschmann, M. (1991). Thermodynamics of multicomponent olivines and the solution properties of $(Ni,Mg,Fe)_2SiO_4$ and $(Ca,Mg,Fe)_2SiO_4$ olivines. *American Mineralogist* **76**, 1232–1248.

Hirschmann, M. M. & Ghiorso, M. S. (1994). Activities of nickel, cobalt, and manganese silicates in magmatic liquids and applications to olivine/liquid and to silicate/metal partitioning. *Geochimica et Cosmochimica Acta* **58**, 4109–4126.

Holzheid, A., Palme, H. & Chakraborty, S. (1997). The activities of NiO, CoO and FeO in silicate melts. *Chemical Geology* **139**, 21–38.

Humayun, M., Qin, L. & Norman, M. D. (2004). Geochemical evidence for excess iron in the mantle beneath Hawaii. *Science* **306**, 91–94.

Huppert, H. E. & Sparks, R. S. J. (1985). Komatiites I: Eruption and flow. *Journal of Petrology* **26**, 694–725.

Jones, J. H. (1984). Temperature- and pressure-independent correlations of olivine/liquid partition coefficients and their application to trace element partitioning. *Contributions to Mineralogy and Petrology* **88**, 126–132.

Kauahikaua, J., Hildenbrand, T. & Webring, M. (2000). Deep magmatic structures of Hawaiian volcanoes, imaged by three-dimensional gravity models. *Geology* **28**, 883–886.

Kelemen, P. B., Hart, S. R. & Bernstein, S. (1998). Silica enrichment in the continental upper mantle via melt/rock reaction. *Earth and Planetary Science Letters* **164**, 387–406.

Kinzler, R. J., Grove, T. L. & Recca, S. I. (1990). An experimental study on the effect of temperature and melt composition on the partitioning of nickel between olivine and silicate melt. *Geochimica et Cosmochimica Acta* **54**, 1255–1265.

Kogiso, T., Hirschmann, M. M. & Reiners, P. W. (2004). Length scales of mantle heterogeneities and their relationship to ocean island basalt geochemistry. *Geochimica et Cosmochimica Acta* **68**, 345–360.

Korenaga, J. & Kelemen, P. B. (2000). Major element heterogeneity in the mantle source of the North Atlantic igneous province. *Earth and Planetary Science Letters* **184**, 251–268.

Leeman, W. P. (1974). Part I, Petrology of basaltic lavas from the Snake River Plain, Idaho; and Part II, Experimental determination of partitioning of divalent cations between olivine and basaltic liquid. Doctoral dissertation thesis, Eugene, OR: University of Oregon.

Leeman, W. P. & Lindstrom, D. J. (1978). Partitioning of Ni^{2+} between basaltic and synthetic melts and olivines—an experimental study. *Geochimica et Cosmochimica Acta* **42**, 801–816.

Li, C. & Ripley, E. M. (2010). The relative effects of composition and temperature on olivine–liquid Ni partitioning: Statistical deconvolution and implications for petrologic modeling. *Chemical Geology* **275**, 99–104.

Lindsley, D. H., Grover, J. E. & Davidson, P. M. (1981). The thermodynamics of the $Mg_2Si_2O_6$–$CaMgSi_2O_6$ join: A review and an improved model. In: Newton, R. C., Navrotsky, A. & Wood, B. J. (eds) *Advances in Physical Geochemistry: Thermodynamics of Minerals and Melts*. New York, NY: Springer, pp. 149–175.

Longhi, J. (2002). Some phase equilibrium systematics of lherzolite melting: I. *Geochemistry, Geophysics, Geosystems* **3**, doi:10.1029/2001GC000204.

Longhi, J., Walker, D. & Hays, J. F. (1978). The distribution of Fe and Mg between olivine and lunar basaltic liquids. *Geochimica et Cosmochimica Acta* **42**, 1545–1558.

Matzen, A. K., Baker, M. B., Beckett, J. R. & Stolper, E. M. (2009). The temperature and pressure dependence of Ni partitioning between olivine and MgO-rich silicate melt. *Geochimica et Cosmochimica Acta* **73**, A851.

Matzen, A. K., Baker, M. B., Beckett, J. & Stolper, E. M. (2010). The temperature and pressure dependence of Ni partitioning between olivine and high-MgO silicate melts. *EOS Transactions American Geophysical Union, Fall Meeting Supplement* **90(52)**, Abstract V13F-03.

Matzen, A. K., Baker, M. B., Beckett, J. R. & Stolper, E. M. (2011). Fe–Mg partitioning between olivine and high-magnesian melts and the nature of Hawaiian parental liquids. *Journal of Petrology* **52**, 1243–1263.

Médard, E., McCammon, C. A., Barr, J. A. & Grove, T. L. (2008). Oxygen fugacity, temperature reproducibility, and H_2O contents of nominally anhydrous piston-cylinder experiments using graphite capsules. *American Mineralogist* **93**, 1838–1844.

Minarik, W. G., Ryerson, F. J. & Watson, E. B. (1996). Textural entrapment of core-forming melts. *Science* **272**, 530–533.

Mysen, B. (2007). Partitioning of calcium, magnesium, and transition metals between olivine and melt governed by the structure of the silicate melt at ambient pressure. *American Mineralogist* **92**, 844–862.

Mysen, B. O. (1978). Experimental determination of nickel partition coefficients between liquid, pargasite, and garnet peridotite minerals and concentration limits of behavior according to Henry's law at high pressure and temperature. *American Journal of Science* **278**, 217–243.

Mysen, B. O. (2006). Redox equilibria of iron and silicate melt structure: Implications for olivine/melt element partitioning. *Geochimica et Cosmochimica Acta* **70**, 3121–3138.

Mysen, B. O. & Kushiro, I. (1979). Pressure dependence of nickel partitioning between forsterite and aluminous silicate melts. *Earth and Planetary Science Letters* **42**, 383–388.

Nabelek, P. I. (1980). Nickel partitioning between olivine and liquid in natural basalts: Henry's law behavior. *Earth and Planetary Science Letters* **48**, 293–302.

Nisbet, E. G., Cheadle, M. J., Arndt, N. T. & Bickle, M. J. (1993). Constraining the potential temperature of the Archaean mantle: A review of the evidence from komatiites. *Lithos* **30**, 291–307.

Niu, Y., Wilson, M., Humphreys, E. R. & O'Hara, M. J. (2011). The origin of intra-plate ocean island basalts (OIB): the lid effect and its geodynamic implications. *Journal of Petrology* **52**, 1443–1468.

Norman, M. D., Garcia, M. O., Kamenetsky, V. S. & Nielsen, R. L. (2002). Olivine-hosted melt inclusions in Hawaiian picrites: equilibration, melting, and plume source characteristics. *Chemical Geology* **183**, 143–168.

O'Neill, H. St. C. & Berry, A. J. (2006). Activity coefficients at low dilution of CrO, NiO and CoO in melts in the system CaO–MgO–Al_2O_3–SiO_2 at 1400°C: Using the thermodynamic behaviour of transition metal oxides in silicate melts to probe their structure. *Chemical Geology* **231**, 77–89.

O'Neill, H. St. C., Berry, A. J., McCammon, C. C., Jayasuriya, K. D., Campbell, S. J. & Foran, G. (2006). An experimental determination of the effect of pressure on the $Fe^{3+}/\sum Fe$ ratio of an anhydrous silicate melt to 3·0 GPa. *American Mineralogist* **91**, 404–412.

Parman, S. W., Grove, T. L., Dann, J. C. & de Wit, M. J. (2004). A subduction origin for komatiites and cratonic lithospheric mantle. *South African Journal of Geology* **107**, 107–118.

Peslier, A. H., Woodland, A. B. & Wolff, J. A. (2008). Fast kimberlite ascent rates estimated from hydrogen diffusion profiles in xenolithic mantle olivines from southern Africa. *Geochimica et Cosmochimica Acta* **72**, 2711–2722.

Press, W. H., Teukolsky, S. A., Vetterling, W. T. & Flannery, B. P. (1992). *Numerical Recipes*. Cambridge University Press.

Priestley, K. & Tilmann, F. (1999). Shear-wave structure of the lithosphere above the Hawaiian hot spot from two-station Rayleigh wave phase velocity measurements. *Geophysical Research Letters* **26**, 1493–1496.

Putirka, K. D. (2008). Thermometers and barometers for volcanic systems. In: Putirka, K. D. & Tepley, F. J., III (eds) *Minerals,*

Inclusions and Volcanic Processes. Mineralogical Society of America and Geochemical Society, Reviews in Mineralogy and Geochemistry **69**, 61–120.

Putirka, K., Johnson, M., Kinzler, R., Longhi, J. & Walker, D. (1996). Thermobarometry of mafic igneous rocks based on clinopyroxene–liquid equilibria, 0–30 kbar. *Contributions to Mineralogy and Petrology* **123**, 92–108.

Putirka, K., Ryerson, F. J., Perfit, M. & Ridley, W. I. (2011). Mineralogy and composition of the oceanic mantle. *Journal of Petrology* **52**, 279–313.

Putirka, K. D., Perfit, M., Ryerson, F. J. & Jackson, M. G. (2007). Ambient and excess mantle temperatures, olivine thermometry, and active vs. passive upwelling. *Chemical Geology* **241**, 177–206.

Qin, L. & Humayun, M. (2008). The Fe/Mn ratio in MORB and OIB determined by ICP-MS. *Geochimica et Cosmochimica Acta* **72**, 1660–1677.

Rhodes, J. M. & Vollinger, M. J. (2004). Composition of basaltic lavas sampled by phase-2 of the Hawaii Scientific Drilling Project: Geochemical stratigraphy and magma types. *Geochemistry, Geophysics, Geosystems* **5**, Q03G13, doi:10.1029/2002GC000434.

Rhodes, J. M. & Vollinger, M. J. (2005). Ferric/ferrous ratios in 1984 Mauna Loa lavas: a contribution to understanding the oxidation state of Hawaiian magmas. *Contributions to Mineralogy and Petrology* **149**, 666–674.

Ringwood, A. E. (1956). Melting relationships of Ni–Mg olivines and some geochemical implications. *Geochimica et Cosmochimica Acta* **10**, 297–303.

Robin-Popieul, C. C. M., Arndt, N. T., Chauvel, C., Byerly, G. R., Sobolev, A. V. & Wilson, A. (2012). A new model for Barberton komatiites: deep critical melting with high melt retention. *Journal of Petrology* **53**, 2191–2229.

Roedder, E. (1983). Geobarometry of ultramafic xenoliths from Loihi Seamount, Hawaii, on the basis of CO_2 inclusions in olivine. *Earth and Planetary Science Letters* **66**, 369–379.

Roeder, P. L. & Emslie, R. F. (1970). Olivine–liquid equilibrium. *Contributions to Mineralogy and Petrology* **29**, 275–289.

Ryabchikov, I. D. (2003). High NiO content in mantle-derived magmas as evidence for material transfer from the Earth's core. *Doklady Earth Sciences* **389A**, 437–439.

Ryerson, F. J. (1985). Oxide solution mechanisms in silicate melts: Systematic variations in the activity coefficient of SiO_2. *Geochimica et Cosmochimica Acta* **49**, 637–649.

Salters, V. J. M., Longhi, J. E. & Bizimis, M. (2002). Near mantle solidus trace element partitioning at pressures up to 3·4 GPa. *Geochemistry, Geophysics, Geosystems* **3**, doi:10.1029/2001GC000148.

Seifert, S., O'Neill, H. St. C. & Brey, G. (1988). The partitioning of Fe, Ni and Co between olivine, metal, and basaltic liquid: An experimental and thermodynamic investigation, with application to the composition of the lunar core. *Geochimica et Cosmochimica Acta* **52**, 603–616.

Shorttle, O. & Maclennan, J. (2011). Compositional trends of Icelandic basalts: Implications for short-length scale lithological heterogeneity in mantle plumes. *Geochemistry, Geophysics, Geosystems* **12**, Q11008, doi:10.1029/2011GC003748.

Smith, P. M. & Asimow, P. D. (2005). Adiabat_1ph: A new public front-end to the MELTS, pMELTS, and pHMELTS models. *Geochemistry, Geophysics, Geosystems* **6**, Q02004, doi:10.1029/2004GC000816.

Snyder, D. A. & Carmichael, I. S. E. (1992). Olivine–liquid equilibria and the chemical activities of FeO, NiO, Fe_2O_3, and MgO in natural basic melts. *Geochimica et Cosmochimica Acta* **56**, 303–318.

Sobolev, A. V., Hofmann, A. W. & Nikogosian, I. K. (2000). Recycled oceanic crust observed in 'ghost plagioclase' within the source of Mauna Loa lavas. *Nature* **404**, 986–990.

Sobolev, A. V., Hofmann, A. W., Sobolev, S. V. & Nikogosian, I. K. (2005). An olivine-free mantle source of Hawaiian shield basalts. *Nature* **434**, 590–597.

Sobolev, A. V., Hofmann, A. W. *et al.* (2007). The amount of recycled crust in sources of mantle-derived melts. *Science* **316**, 412–417.

Stolper, E., Sherman, S., Garcia, M., Baker, M. & Seaman, C. (2004). Glass in the submarine section of the HSDP2 drill core, Hilo, Hawaii. *Geochemistry, Geophysics, Geosystems* **5**, Q07G15, doi:10.1029/2003GC000553.

Sugawara, T. (2000). Empirical relationships between temperature, pressure, and MgO content in olivine and pyroxene saturated liquid. *Journal of Geophysical Research* **105**, 8457–8472.

Sugawara, T. & Akaogi, M. (2003). Calorimetric measurements of fusion enthalpies for Ni_2SiO_4 and Co_2SiO_4 olivines and application to olivine–liquid partitioning. *Geochimica et Cosmochimica Acta* **67**, 2683–2693.

Takahashi, E. (1978). Partitioning of Ni^{2+}, Co^{2+}, Fe^{2+}, Mn^{2+} and Mg^{2+} between olivine and silicate melts: compositional dependence of partition coefficient. *Geochimica et Cosmochimica Acta* **42**, 1829–1844.

Toplis, M. J. (2005). The thermodynamics of iron and magnesium partitioning between olivine and liquid: criteria for assessing and predicting equilibrium in natural and experimental systems. *Contributions to Mineralogy and Petrology* **149**, 22–39.

Tormey, D. R., Grove, T. L. & Bryan, W. B. (1987). Experimental petrology of normal MORB near the Kane Fracture Zone: 22°–25°N, mid-Atlantic ridge. *Contributions to Mineralogy and Petrology* **96**, 121–139.

Viljoen, R. P. & Viljoen, M. J. (1969). Evidence for the composition of the primitive mantle and its products of partial melting from a study of the mafic and ultramafic rocks of the Barberton Mountain Land. *Geological Society of South Africa Special Publication* **2**, 275–295.

Vogt, J. H. L. (1923). Nickel in igneous rocks. *Economic Geology* **18**, 307–353.

Vokurka, K. & Rieder, M. (1987). Thermal expansion and excess volumes of synthetic olivines on the Mg_2SiO_4–Ni_2SiO_4 join. *Neues Jahrbuch für Mineralogie, Monatshefte*, 97–106.

Walter, M. J. (1998). Melting of garnet peridotite and the origin of komatiite and depleted lithosphere. *Journal of Petrology* **39**, 29–60.

Wang, Z. & Gaetani, G. A. (2008). Partitioning of Ni between olivine and siliceous eclogite partial melt: experimental constraints on the mantle source of Hawaiian basalts. *Contributions to Mineralogy and Petrology* **156**, 661–678.

Wasylenki, L. E., Baker, M. B., Kent, A. J. R. & Stolper, E. M. (2003). Near-solidus melting of the shallow upper mantle: partial melting experiments on depleted peridotite. *Journal of Petrology* **44**, 1163–1191.

Wei, K., Trønnes, R. G. & Scarfe, C. M. (1990). Phase relations of aluminum-undepleted and aluminum-depleted komatiites at pressures of 4–12 GPa. *Journal of Geophysical Research* **95**, 15817–15827.

Wood, B. J. (1974). Crystal field spectrum of Ni^{2+} in olivine. *American Mineralogist* **59**, 244–248.

Wright, T. L. (1984). Origin of Hawaiian tholeiite: a metasomatic model. *Journal of Geophysical Research* **89**, 3233–3252.

Yaxley, G. M. (2000). Experimental study of the phase and melting relations of homogeneous basalt + peridotite mixtures and implications for the petrogenesis of flood basalts. *Contributions to Mineralogy and Petrology* **139**, 326–338.